Preparation and Properties of Elastomer Composites Containing "Graphene"-Based Fillers: A Review

Alice Pazat, Claire Barrès, Florence Bruno, Claude Janin, Emmanuel Beyou

Polymer Reviews

ISSN: 1558-3724 (Print) 1558-3716 (Online) Journal homepage: https://www.tandfonline.com/loi/lmsc20

Preparation and Properties of Elastomer Composites Containing "Graphene"-Based Fillers: A Review

Alice Pazat, Claire Barrès, Florence Bruno, Claude Janin & Emmanuel Beyou

To cite this article: Alice Pazat, Claire Barrès, Florence Bruno, Claude Janin & Emmanuel Beyou (2018) Preparation and Properties of Elastomer Composites Containing "Graphene"-Based Fillers: A Review, Polymer Reviews, 58:3, 403-443, DOI: 10.1080/15583724.2017.1403446

To link to this article: https://doi.org/10.1080/15583724.2017.1403446

Published online: 18 Jan 2018.

POLYMER REVIEWS
2018, VOL. 58, NO. 3, 403–443
https://doi.org/10.1080/15583724.2017.1403446

Taylor & Francis
Taylor & Francis Group

REVIEW

Preparation and Properties of Elastomer Composites Containing "Graphene"-Based Fillers: A Review

Alice Pazat[a,b], Claire Barrès[c], Florence Bruno[b], Claude Janin[b], and Emmanuel Beyou[a]

[a]Univ Lyon, Univ Lyon 1, CNRS UMR 5223, Ingénierie des Matériaux Polymères, Villeurbanne, France; [b]Laboratoire de Recherches et de Contrôle du Caoutchouc et des Plastiques, LRCCP, Vitry-sur-Seine cedex; [c]Univ Lyon, INSA Lyon, CNRS UMR 5223, Ingénierie des Matériaux Polymères, Villeurbanne, France

ABSTRACT

Elastomers are materials showing exceptional elasticity and are used for numerous applications. However, their low stiffness as well as their insulating behavior can be limiting so the incorporation of graphene-based materials can help and improve drastically their properties. With high Young's modulus, high electrical and thermal conductivities, graphene and graphene-like fillers seem ideal fillers to effectively tune elastomers properties. With low graphene-like loadings, most elasticity properties of elastomers could be preserved while increasing or adding new properties to the composites to enable new applications. Herein, we focus on the effects of "graphene" incorporation into elastomers and we will highlight the key parameters to effectively monitor the changes.

KEYWORDS

Graphene; elastomer; properties

1. Introduction

Much research interest has been focused on graphene since the attribution of a Nobel Prize in Physics to Andre Geim and Konstantin Novoselov from Manchester University (UK) in 2010.[1–4] Indeed, graphene is of great scientific interest due to its outstanding properties in comparison with other common fillers such as silica, clays, and carbon nanotubes. Indeed, a single graphene sheet has a Young's modulus of 1 TPa and a yield strength of 130 GPa which makes it the toughest material ever measured.[2] Besides, graphene has a thermal conductivity of 5000 W/m.K, about 12 times higher than copper and its electrical conductivity properties are also outstanding with 128 S/m^2 and charge mobility around 200 S.m^2/C, hence 45,000 times higher than copper. In addition, due to its 2D dimension, graphene has a very high theoretical specific surface area (2,630 m^2/g) as well as a very low permeability to most gases including helium. Thus, even if helium has a small kinetic diameter of 2.6 Å, graphene has an even lower pore diameter as well as a high penetration energy barrier of 18.8 eV (compared to 18.6 eV kinetic energy for a helium atom).[3] In addition, graphene is a flexible, tough material exhibiting good optical transparency properties.[4] The expectations about the exceptional theoretical properties of this material have led many researchers to work upon

CONTACT Emmanuel Beyou beyou@univ-lyon1.fr Univ Lyon, Univ Lyon 1, CNRS UMR 5223, Ingénierie des Matériaux Polymères, F-69622 Villeurbanne, France.

Color versions of one or more of the figures in the article can be found online at www.tandfonline.com/lmsc.

isolation of single graphene sheets. Nowadays industrial production of graphene-based materials (GBMs) is developing with many start-up companies appearing on the market. Yet, many efforts are still to be made for large quantities of defect-free graphene sheets to be produced at reasonable costs.[5–15]

Applications of this material are wide and include electronics, photovoltaics, and energy storage as well as high-performance composites. For the latter, polymers have shown to be of great interest to produce easily processable materials with enhanced thermal or mechanical properties for instance. GBMs could be used as additional fillers or as a replacement of traditional reinforcing fillers such as carbon black (CB). Besides, they are expected to enhance properties such as thermal and electrical conductivities even at a very low loading (< 1 wt%). Regardless of the application it is necessary to ensure appropriate dispersion of this filler in a polymer matrix because its small dimension as a single layer is of great interest since large surface areas are available to interact with the matrix. However, the strong π-π stacking interactions cause the combination of graphene layers. To avoid such phenomenon, many functionalization strategies have been developed over the past years.[16,17] They include non-covalent[18–27] and covalent[28–46] attachment. Non-covalent modification of graphene sheets is an efficient way to tune its properties while preserving its conjugated structure. It includes π-π interactions, hydrophobic attraction between a surfactant and graphene sheets, and hydrogen bonding.[47,48] For example, poly-aromatic hydrocarbons such as naphthalene, anthracene, and pyrene functionalized with side chains were effective.[49,50] Moreover, surfactants and ionic liquids were used for wrapping graphene sheets.[52,53]

However, covalent functionalization through the use of the redox method is most widely reported since the presence of oxygen functional groups on the surface and edges of an oxidized form of graphene sheets allows for very diverse chemical reactions to take place and then opens a wide range of available routes for functionalization.[54–78] In addition, through several reduction treatments, the graphene oxide sheets can be converted back to a GBM.[79–103] This oxidation/reduction method is of considerable interest for the industry as it might open the way for large production of GBMs at low costs. Hence, while defect-free graphene layers can be prepared through expensive chemical vapor deposition (CVD) process,[104] the redox method is mostly a chemical process using low-cost graphite as a starting material. However, these fillers, having a lateral dimension/thickness less than 100 nm and often called graphite nanoplatelets (GNPs), show inferior performances in terms of several performances such as electrical conductivity. These GNPs anyhow enable the development of polymer nanocomposites. Even if they show lower properties than defect-free graphene, they however retain the ability to enhance mechanical properties, electrical and thermal conductivities as well as barrier properties of polymer composites. Among common polymers, elastomers are amorphous polymers with very flexible chains, thus possessing glass transition temperatures below ambient temperatures. In their current uses, they are therefore in the rubbery state and exhibit a soft solid-like behavior with high deformability. However, to be able to withstand large deformations and recover their original configuration when the stress is removed, *i.e.*, to exhibit rubber elasticity, elastomers have to be crosslinked. Rubbers are widely used for their exceptional elasticity and damping properties.[105] Current elastomers are used in their crosslinked form, and are then referred to as vulcanizates. For clarity, in this review, the term elastomer will be preferred to refer to the polymer

matrix, whereas rubber will more generally indicate the crosslinked material, except when naming the elastomers according to the common nomenclature and abbreviations (for example, NR, which stands for natural rubber, *i.e.*, natural polyisoprene). Some polymeric systems exhibit similar hyperelastic properties while not requesting crosslinking. They are copolymers or blends in which a physical network exists and reversibly vanishes upon heating, allowing the same processing routes as thermoplastics. Therefore, these materials are called thermoplastic elastomers or TPEs. They are often reinforced with low cost CB to enhance mechanical properties such as tensile strength.[106–109] However, it is usually necessary to use high loadings (>25 wt%) leading thus to important reduction in strain at break. The use of graphene sheets, and more generally of GBMs could enable an increase in tensile strength while preserving strain at break of the elastomers. Besides, electrical and thermal conductivities could be induced, still with a low loading. Eventually, due to their platelet structure, GBMs have a great potential in increasing barrier properties of elastomers.

2. Preparation of elastomer-based composites

2.1 Filler dispersion: Mechanisms and difficulties

To be efficient, fillers need to be well dispersed in the elastomer and so they require good filler matrix compatibility. They need to interact with the polymer matrix through physical and or chemical linkages. Those interactions depend upon various parameters such as filler morphology, size, and surface activity. To be well reinforcing, they need to be of small size to form a colloidal suspension within the matrix.[110] It is known that large particles (>5 μm) tend to degrade elastomeric properties, creating local heterogeneities that are often the starting points for cracks. Smaller particles (between 1 and 5 μm) are reported to be compatible with elastomers without being able to strongly reinforce the material. Thus, particle sizes smaller than 1 μm are often looked for.[106] A well-dispersed nanosized filler would be of great interest since it would provide a large interfacial area and would lower the average distance between particles in a composite. These properties allow for a lower loading and so enable to reduce weight and keep high elasticity.[111]

Elastomers are highly viscous materials that need to be well mixed to be able to obtain an adequate dispersion of the filler in the matrix, in order to reach the desired properties for the final compound.

This means that through the mixing process large agglomerates (up to 1 mm for carbon black) need to be broken.[106] Mixing of elastomers is often reported to occur in three main stages: incorporation of the additives, a dispersive mixing step, and a distributive mixing step.[112] Figure 1 shows the difference between a dispersive and a distributive mixing for CB.

During the dispersive step, large components undergo size reduction by separation through erosion and rupture of the agglomerates in smaller fragments that are then separated in the matrix.[113,114] The last step distributes the small fragments in the matrix without affecting their physical form.[114] These two last phases however do not necessarily happen one after another but most likely happen rather simultaneously.

Dispersion mechanisms of CB agglomerates are reported to occur through (i) rupture, a sudden fracture of the pellets into a few fragments and (ii) erosion, a progressive mechanism where small fragments are continuously detached from the periphery of the agglomerate.[113,114]

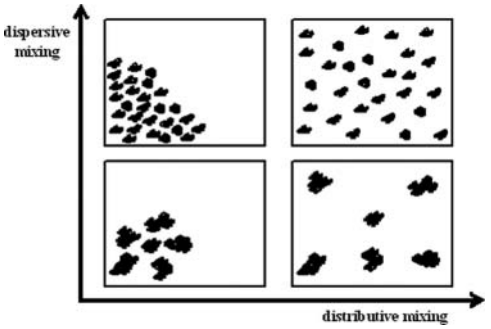

Figure 1. Representation of dispersive and distributive mixing processes for CB in elastomers.

Rupture occurs above a critical shear stress when hydrodynamic forces exceed cohesive forces, which depend on the CB pellet size. Erosion, on the contrary, proceeds through the detachment of a fixed eroded volume per strain unit and is driven by the applied shear stress and strain. It is a local mechanism whose rate depends on the CB properties. Hence, faster erosion has been reported for CB with high structures.[113]

Lamellar nanofillers dispersion occurs through different mechanisms. Ideal dispersion of platelets-like fillers requires complete exfoliation, which means that all layers should be apart from each other. The main problem to achieve such dispersion is the strong interlayer interactions that need to be overcome in order to separate the layers. Clays such as montmorillonite (MMT) have attracted much research attention over the past few years and the exfoliation mechanisms of these materials have been studied. A major breakthrough in MMT dispersion was the development of intercalation techniques to enable a reduction in the interlayer interactions and thus to facilitate exfoliation. Another main development in MMT exfoliation in a polymer matrix was based on MMT surface modification to lower surface energy and to enhance filler-matrix interactions.[118]

Less work has been reported on GNPs dispersion. However, the similarities in morphology with MMT led many groups to apply similar procedures. The use of intercalated and expanded compounds has thus been reported as well as chemical modification of the graphene sheets surface to decrease the strong π-π interactions between layers.[119] Naming the resulting GBMs needs to be developed to avoid misunderstandings between the scientific community so that Bianco et al.[13] and Wick et al.[120] described various derivatives of graphene and a classification grid for the different graphene forms according to their number of graphene layers, their average lateral dimension, and their atomic carbon/oxygen ratio was established (Fig. 2a).

Moreover, few-layer graphene (FLG) corresponds to the 2–5 sheet material while the multi-layer graphene (MLG) one consists of 6–10 stacked graphene layers.[119] On the other hand, graphene oxide refers to a monolayer of a chemically modified graphene sheet prepared by oxidation and exfoliation while graphite oxide (GO acronym, herein) is a bulk solid material made by oxidation of graphite (Fig. 2a).

Figure 2b is a representation of stacked, expanded, and exfoliated graphite platelets in an elastomeric matrix. Exfoliation of GNPs into an elastomer is desired to enhance the properties of the final material. Most exfoliation processes are performed in suspension rather than during bulk processing, during which, high shear is reported to break the platelets rather than to exfoliate them.[119]

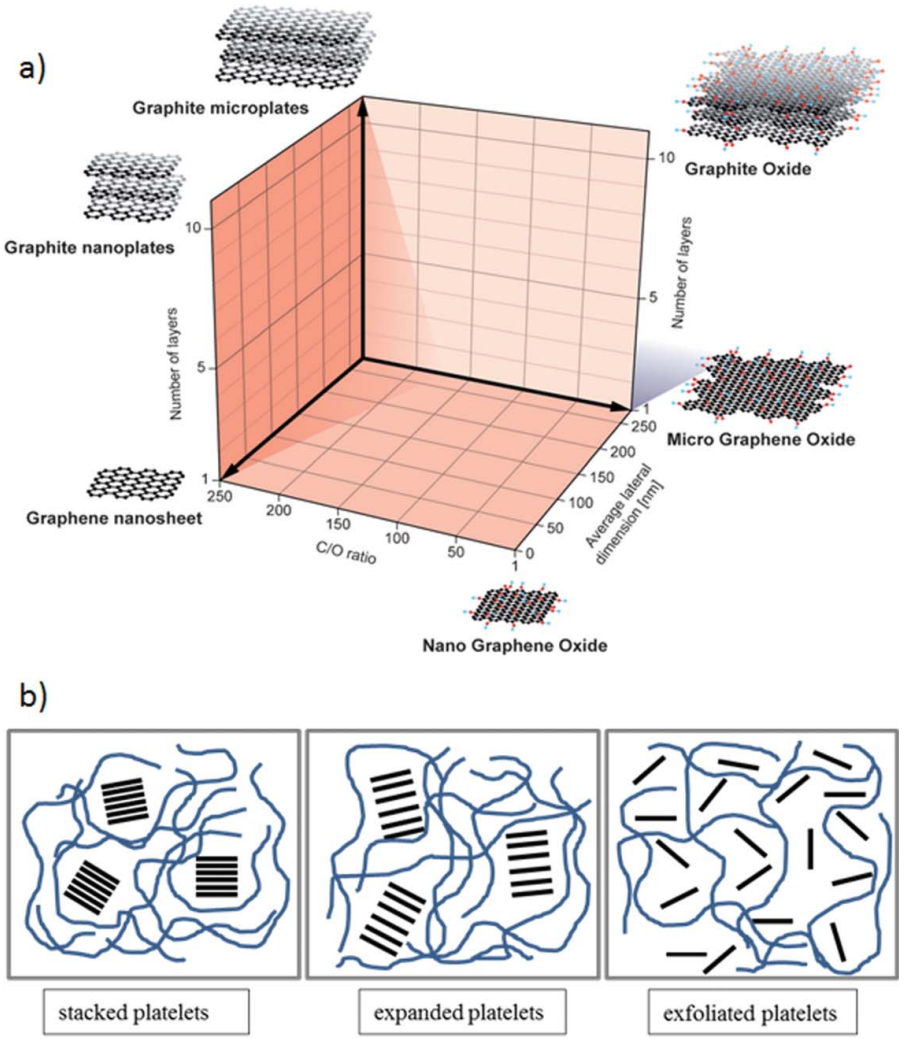

Figure 2. (a) Classification grid for the different graphene forms according to their number of graphene layers, their average lateral dimension, and their atomic carbon/oxygen ratio. The different materials drawn at the six corners of the box represent the ideal cases. Reproduced with permission from[120] Copyright 2014, Wiley. (b) Dispersion states of graphite fillers in an elastomer matrix.

2.2 Mixing techniques

2.2.1 Solution blending

Solution blending, which consists in dissolving the elastomer in an appropriate solvent and adding all fillers and additives in the mixture, is very common for research purposes.[6,121–123] It is often observed to lead to homogeneous dispersion of the fillers, added in suspension in a solvent in the dissolved polymer. However, it requires long time (several hours) to dissolve the elastomer and the use of large quantities of toxic organic solvents such as toluene, which have to be fully evaporated to recover the solid compound: this is not desirable in industry. Besides, a less described process is the synthesis of the elastomer in the presence of the

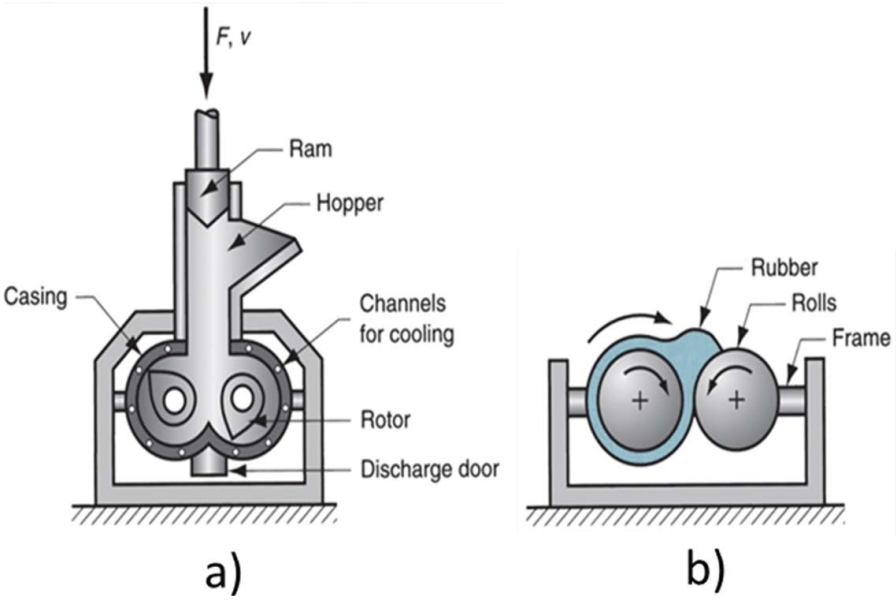

Figure 3. Bulk mixing apparatus: (a) internal mixer and (b) two-roll mill.

fillers.[6] This is however mainly applicable for research studies. Other techniques such as *in situ* polymerization have also been reported and will not be detailed here.

2.2.2 Bulk mixing

Industrially, elastomers are mostly processed through so-called "direct blending." Compounding is carried out in an internal mixer consisting in a bi-cylindrical chamber closed by a ram and containing tangential or interpenetrating rotors. In a second step, the mix is discharged on a two-roll mill for further homogenization and cooling. Processing equipment is shown in Fig. 3.

In an internal mixer, gum and additives are fed from the hopper and the ram comes down to close the chamber containing the rotors.[124] The mix is then discharged at the bottom of the equipment. In a two-roll mill, the elastomer sticks to one roll and forms a bead between the two counter-rotative rolls. A sheet can be formed, which will be then transformed in bands or preforms to feed the process giving its final shape to the product, prior to crosslinking. However, this process is often reported to lead to less homogenous dispersion and distribution of graphite nanofillers inside an elastomeric matrix than solution-blending technique. Moreover, high shear forces usually applied to overcome the high viscosity of the elastomeric matrix can lead to the breakage of the graphene sheets.[119]

2.2.3 Latex compounding

Mixing of elastomers in latex phase is also commonly used in the industry. Natural rubber (NR) exists naturally in latex form (30–40 wt% solid content) and nitrile butadiene rubber (NBR) can be synthesized in latex form. Through the use of appropriate equipment such as a high-shear mixer, it is possible to disperse fillers and other additives in an elastomeric matrix in the aqueous phase. At a laboratory scale, it is often done by adding an aqueous suspension of the filler in a latex under mechanical stirring, sonication, or the use of a

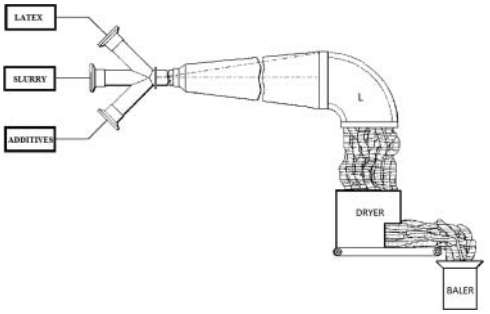

Figure 4. Equipment for latex processing. Adapted from[125].

high-shear mixer. At an industrial scale, high speed units are used and do not always require mechanical stirring of the latex with the filler, as shown in Fig. 4.[125]

A Cabot Corporation patent describes a process to mix an elastomer latex with CB and additives.[125] First, an aqueous suspension of CB ("slurry") is prepared and homogenized in several mixing units. A latex is slowly fed (1.5 $m.s^{-1}$) in the coagulum reactor at about atmospheric pressure. Additives are discharged in the latex, then the carbon black slurry is pushed into this medium at high speed (150 $m.s^{-1}$) and under high pressure (70 bars). Spontaneous coagulation of the latex occurs. In many processes, addition of an aqueous acid or salt solutions is often reported to be necessary to coagulate the latex mix. In a last step, the coagulum is dried in an extruder to remove water and it is finally compacted into bales.

Other processes involving coagulation of the latex after shaping the product ("dipping process," for example) are also common in the industry, for gloves manufacturing, for example.

3. Properties of elastomer/graphene-based composites

3.1 Barrier properties

3.1.1 Permeability

Rubber nanocomposites can be of great interest for sealing and tightness applications, for example, in tires, buildings, and hydraulic systems. Elastomers contain a large free volume and so are highly permeable to most gases.

Transport properties of small molecules such as gases through elastomers usually occur in three main steps: (i) adsorption of molecules onto the upstream side of the polymer membrane, (ii) dissolution and diffusion of the permeant inside the matrix, and (iii) desorption of gas molecules from the downstream side of the membrane (Fig. 5).[126,127]

Transport properties thus depend on the affinity of the diffusion molecule for the elastomer membrane as well as the mobility of the permeant inside the matrix. Adsorption and desorption of the gas molecules onto and from the surface are considered very fast and the rate-limiting step in transport of gas molecules though a matrix is the dissolution-diffusion step.[128] The driving force for the diffusion of gas molecules into an elastomer is the presence of a concentration gradient in gas molecules between the two surfaces of an elastomer membrane. Gas molecules diffuse from areas of high concentrations to areas of low concentration until equilibrium is reached. The diffusion phenomenon is often described by Fick's law

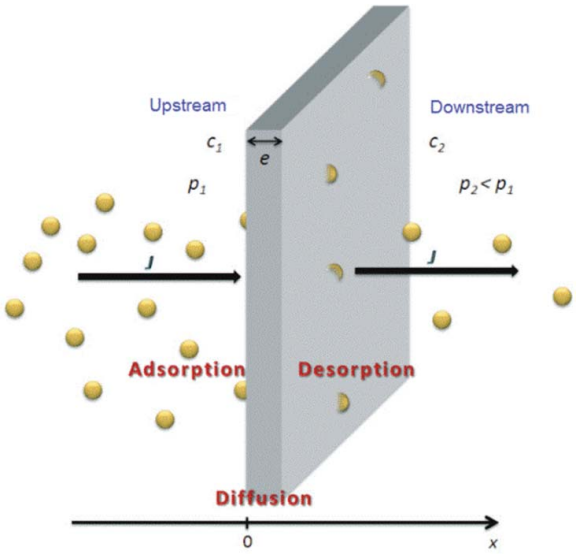

Figure 5. Schematic representation of steps in molecular transport through a membrane. Adapted from.[128]

(Eq. 1), describing the linear diffusion of a molecule through a membrane.[126]

$$J = -D\frac{\partial c}{\partial x} \tag{1}$$

where J is the flow in diffusing molecules by unit of time and area ($cm^3_{STP}.cm^{-2}.s^{-1}$), c is the local volume concentration in diffusing molecules (cm^3_{STP}), and D is the diffusion coefficient ($cm^2.s^{-1}$) with STP standing for standard temperature and pressure.

In a Fickian diffusion process, the main parameters affecting transport properties of small molecules through a membrane are related according to Eq. (2).

$$P = D \times S \tag{2}$$

where P is the permeability coefficient ($cm^3_{STP}.cm.cm^2.s.cmHg$ or also expressed in $mol.m.m^2.s^{-1}.Pa^{-1}$), D is the diffusion coefficient ($cm^2.s^{-1}$), and S is the solubility coefficient ($cm^3_{STP}.cm^{-3}.cm_{Hg}$).

The permeability coefficient P characterizes the ability of the gas molecules to go through an elastomeric membrane when a pressure gradient is applied (Eq. 3).

$$P = \frac{e \times J}{(p_1 - p_2)} \tag{3}$$

where e is the thickness (cm, considered constant), p_1 is the upstream partial pressure (cm_{Hg}), and p_2 is the downstream partial pressure (cm_{Hg}).

The diffusion coefficient characterizes the ability of the permeant to go through the matrix and the solubility coefficient is related to the affinity of the permeant for the matrix. Several factors influence transport of gas molecules through an elastomeric membrane such as (i)

environmental factors such as temperature, pressure, concentration, (ii) intrinsic properties of the elastomer such as free volume and glass transition temperature (related to the chain mobility), (iii) the presence of plasticizers, and (iv) the affinity of gas molecules for the elastomer.[127,128]

3.1.2 Permeability mechanisms and models in nanocomposites

The addition of impermeable fillers can enhance the barrier properties of the elastomer matrix. Defect-free graphene is impermeable to all gases including helium and it is thus an ideal candidate to effectively reduce permeability of rubber composites.[129–135] While GBMs are not fully impermeable to gases, they however retain elevated barrier properties to most gases. For example, Ha et al.[136] reported a 35% decrease in permeability toward nitrogen, oxygen, hydrogen, methane, and carbon dioxide gases for graphite oxide/polydimethysiloxane-based composites at a 1 wt% GO content. Many parameters such as filler shape, size, orientation, and dispersion in the host matrix play a significant role in barrier properties of nanocomposites. Platelet-like nanofillers are the most promising since they are able to form a tortuous path to effectively slow down the diffusion of gas molecules inside the material, as illustrated in Fig. 6.

Hence, at 5 phr (weight parts per hundred parts of the polymer matrix) loading in styrene-butadiene rubber (SBR), Song et al.[130] reported a 35% decrease in permeability of composites containing low defect graphene (exhibiting a platelet morphology), as compared to composites with CB, whose aspect ratio is much lower.

Several models can be used to describe permeability as a function of the filler content.[3,123,137–143] Nielsen's model[138] is the most common one and it is also referred to as "classic tortuosity model." It assumes that impermeable flakes with a certain aspect ratio associated with their cross-section are uniformly dispersed in a permeable matrix.[3] Nielsen's model can be written according to Eq. (4).

$$\frac{P}{P_0} = \frac{1-\Phi}{1+\tau} \tag{4}$$

where P is the gas permeability of the composite, P_0 is the gas permeability of the pure polymer matrix, Φ is the volume fraction of the filler, and τ is the tortuosity factor. P/P_0 is called the relative permeability. This model assumes random orientation of the fillers in the matrix, ignoring the significantly different behavior of aligned platelets.

According to the model used, the tortuosity factor will have a different expression. In Nielsen's classical model, it is expressed as Eq. (5).

$$\tau = \frac{\alpha}{2}\Phi \tag{5}$$

with α the aspect ratio of the filler.[138]

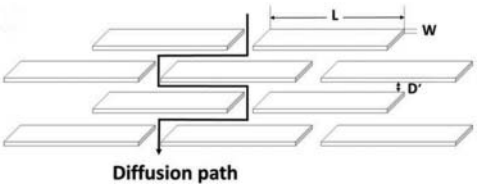

Figure 6. Gas diffusion path inside the material. Adapted from[3].

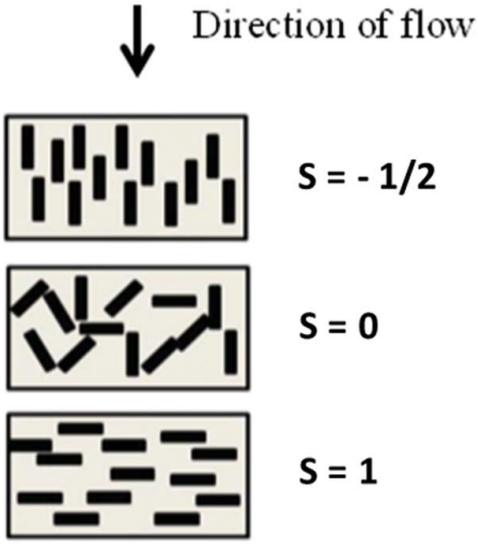

Figure 7. Filler orientations according to the Bharadwaj model. Adapted from[3].

Cussler et al.[142] proposed a model similar to Nielsen's in which two different tortuosity factors were added: one for random alignment of the fillers and another one for perfectly aligned fillers.[123,142] Another attempt to include filler orientation in the composite has been done by Bharadwaj[139] who included *S*, an orientation parameter equal to a value of −0.5 for parallel orientation (no tortuosity), 0 for random orientation and 1 for perpendicular alignment of the platelets in the material, as shown in Fig. 7.

Bharadwaj's equation with tortuosity factor can then be expressed as Eq. (6).

$$\frac{P}{P_0} = \frac{(1-\Phi)}{1 + \frac{\alpha}{2}\Phi + \frac{2}{3}\left(S + \frac{1}{2}\right)\Phi} \tag{6}$$

It is very similar to Nielsen's model but is more versatile as it takes into account more parameters to fit the system. From Fig. 7, it is suggested that alignment of the platelets perpendicular to the flow will create greater tortuosity and thus will increase the diffusion length of the permeant in the composite.

Other models such as Gusev-Lusti,[140] and Fredrickson and Bicerano[141] also exist but they will not be extensively presented here. It was shown by Dunkerley and Schmidt[143] that most models provide similar results at low filler content (<10 vol%). With most studies on graphitic fillers being performed at low loadings (under 10 vol%), any of these models can be used.

3.1.3 Influence of filler size, shape, and aspect ratio

A high aspect ratio of the filler is of significant importance since large fillers will divert more the diffusion path and so will increase the total path length, as shown in Fig. 6. This leads to reduced permeability of the material. It was shown by Ozbas et al.[122] that increased surface area of thermally reduced graphene oxide flakes (referred to as "functionalized graphene

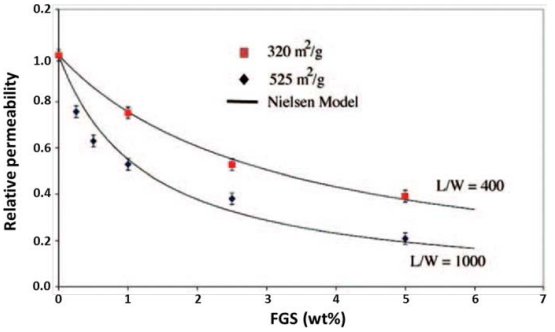

Figure 8. Reduction in air permeability as a function of functionalized graphite sheets (FGS) loading in PDMS (as compared to neat PDMS). Solid lines represent Nielsen's model predictions. L/W is the aspect ratio (length/width) of the filler particles in the sample. Reproduced with permission from[122] Copyright 2012, Wiley.

sheets," FGS) led to more efficient barrier properties of polydimethylsiloxane (PDMS)-based composites as displayed in Fig. 8.

The FGS sample with the highest aspect ratio provides the lowest permeability. These plots show the decrease in air permeability of PDMS-FGS composites with increasing filler loading, with FGS fillers exhibiting different specific surface area, associated with different aspect ratios of the particles (L/W).[122] 60% and 80% decrease in air permeability were reached for FGS exhibiting a specific surface area of 320 m^2/g and 525 m^2/g, respectively, at 5 wt% loading in PDMS matrix. This emphasizes the significant effect of filler aspect ratio on the barrier properties of the corresponding composites. Besides, Ozbas et al.[122] observed a fine fit of Nielsen's curve with their experimental values. Moreover, Yoo et al.[3] investigated the effect of aspect ratio, orientation and aggregation of graphene or GO over the oxygen permeability. The calculations confirmed that a high aspect ratio is preferred to decrease the permeability of the composites, as shown in Fig. 9.

At 1 vol% of graphene-based fillers, by increasing the aspect ratio (α) of the platelets from 30 to 3000, the relative permeability of the composites with respect to the neat matrix decreased by 10 % and 90 %, respectively, showing the major effect of filler aspect ratio over permeation properties (Fig. 9a). Figure 9b shows the decrease in permeability of the composites as a function of graphene loading for various numbers of layers (N). For perpendicular orientation ($S = 1$, Figs. 7 and 9b), a single layer of graphene ($N = 1$) will provide a decrease in permeability greater than 90 % while for a stack of 10 layers ($N = 10$, lower aspect ratio), a value of only 60 % can be reached (Fig. 9b). While well exfoliated platelets create a very tortuous path, stacks of nanosheets will significantly reduce the diffusion path. At the same volume fraction, the probability for a gas molecule to meet a graphene nanoplatelet will be lowered if the stacking parameter (N, number of layers) is high.[3]

3.1.4 Influence of filler orientation

The influence of filler orientation on the permeability of the composites was also computed by Yoo et al.[3] Perpendicular orientation of the platelets ($S = 1$) showed superior permeability reduction than the randomly oriented ones, as displayed in Fig. 9b. The former configuration led to 60% decrease in oxygen permeability whereas the latter only reached 35% reduction for 10 layer-nanoplatelets at 1 vol% loading, as compared to the pure polymer. The main

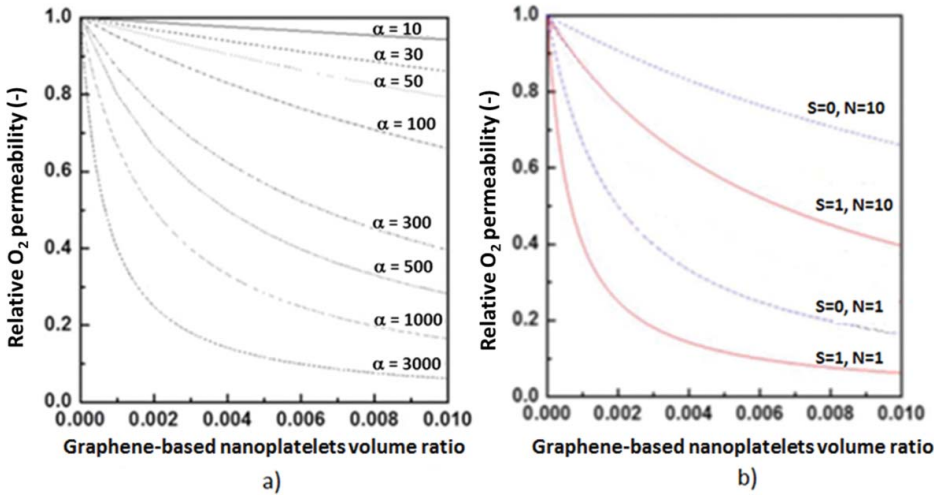

Figure 9. (a) Effect of graphene-based nanoplatelets aspect ratio on the O_2 permeability of a polymer matrix and (b) influence of the graphene-based nanoplatelets orientation and stacking on O_2 permeability. Adapted from[3].

factor in improving barrier properties is then tortuosity. For perpendicular orientation ($S = 1$), tortuosity is maximized and, therefore, this configuration is the most effective one in increasing the diffusion path of gas molecules inside the composite.

These studies have shown the effect of filler shape, size, and aspect ratio, on permeability. Besides, filler orientation has proven to be of significant influence on permeability of the composites. This feature is much related to processing. Several research groups thus investigated the influence of processing conditions, and composites morphologies, on barrier properties of elastomer composites.

3.1.5 Influence of processing and functionalization

Table 1 highlights the main results in gas barrier properties comparing the processing methods, the GBMs loadings, and the elastomer matrix.

Kim et al.[129] showed that the same TRG filler, dispersed according to three different routes, resulted in three distinct behaviors in permeation. The main permeation results of their study are shown in Fig. 10.

Figure 10 shows a decrease in relative permeability to nitrogen gas as a function of the volume fraction of several GBMs in TPU composites. The influence of processing can be seen. Hence, composites with 1.6 vol% of TRG prepared through direct melt mixing led to a 50% decrease in nitrogen gas permeability while *in situ* polymerized composites induced a 70% decrease. Solution-blended samples at the same loading were even more efficient (up to 80% permeability reduction).[129] In addition, the effects of surface functionalization and processing route obviously result in variations of the state of dispersion of the filler, which is a key factor regarding the composite properties. Thus, morphologies of the composites provide some understanding of the permeability results. Figure 11 shows TEM images of TPU composites containing GBMs.

Figure 11a shows the morphology of melt-compounded composites containing graphene-based aggregates of at least 1.5 μm in length while the materials containing TRG (Figs. 11b

Table 1. Short literature review of gas permeability data of GBMs/elastomer composites[a].

Filler	Loading	Matrix	Processing	Permeant	Relative reduction (in comparison with pristine polymer)	Reference
Low defect graphene flakes	5 phr	SBR	Latex	O_2	−35%	122
rGO	4 phr	NR	Latex	O_2	−70%	123
rGO	4 phr	NR	Latex + two-roll mill	O_2	−30%	123
Graphite	1.6 vol%	TPU	Solution Melt *in situ* polymerization	N_2	−5%	119
TRG	1.6 vol%	TPU	Melt mixing	N_2	−50%	119
TRG	1.6 vol%	TPU	*In situ* polymerization	N_2	−70%	119
TRG	1.6 vol%	TPU	Solution	N_2	−80%	119
GO	1.6 vol%	TPU	*In situ* polymerization	N_2	−60%	119
Phenyl isocyanate – GO	1.6 vol%	TPU	Solution	N_2	−98%	119
Acetyl phenyl isocyanate –GO	1.6 vol%	TPU	Solution	N_2	−94%	119
Exfoliated graphite (using microwaves)	10 phr	NR	Latex + HAAKE + two-roll-mill	N_2	−38%	125

[a]Acronyms used: rGO (reduced graphite oxide); TRG (thermally reduced graphite oxide); SBR (styrene-butadiene rubber); NR (natural rubber); TPU (thermoplastic polyurethane).

and 11c) display a rather uniform distribution. TRG particles incorporated through solution blending (Fig. 11d) or *in situ* polymerization (Figs. 11e and 11f) look slightly more uniformly distributed in the matrix. The performance of the composite in permeation seems to be directly related to the state of dispersion. Indeed, solution-blended TRG (Fig. 11d) are more homogeneously dispersed in the TPU matrix and lead to better barrier properties of the composites. In addition, the effect of surface functionalization was investigated by comparing morphologies of composites containing pristine or modified GO. Images of GO-based composites (Fig. 11i) and modified GO-based composites (Figs. 11g and 11h) reveal thinner aggregates than TRG and suggest interconnection between fillers.[129] Phenylisocyanate and acetylphenyl isocyanate-functionalized GO appear to be rather uniformly dispersed in the matrix. They also display the largest decrease of permeability (−98% and −94%, respectively). Thanks to its effect on dispersion, functionalization can thus be an efficient way to

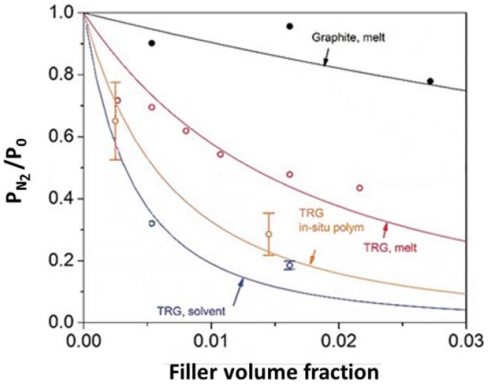

Figure 10. N_2 permeability of TPU composites as a function of the GBMs content. Solid lines are predictions according to the model of Lape et al.[123] Adapted from[129].

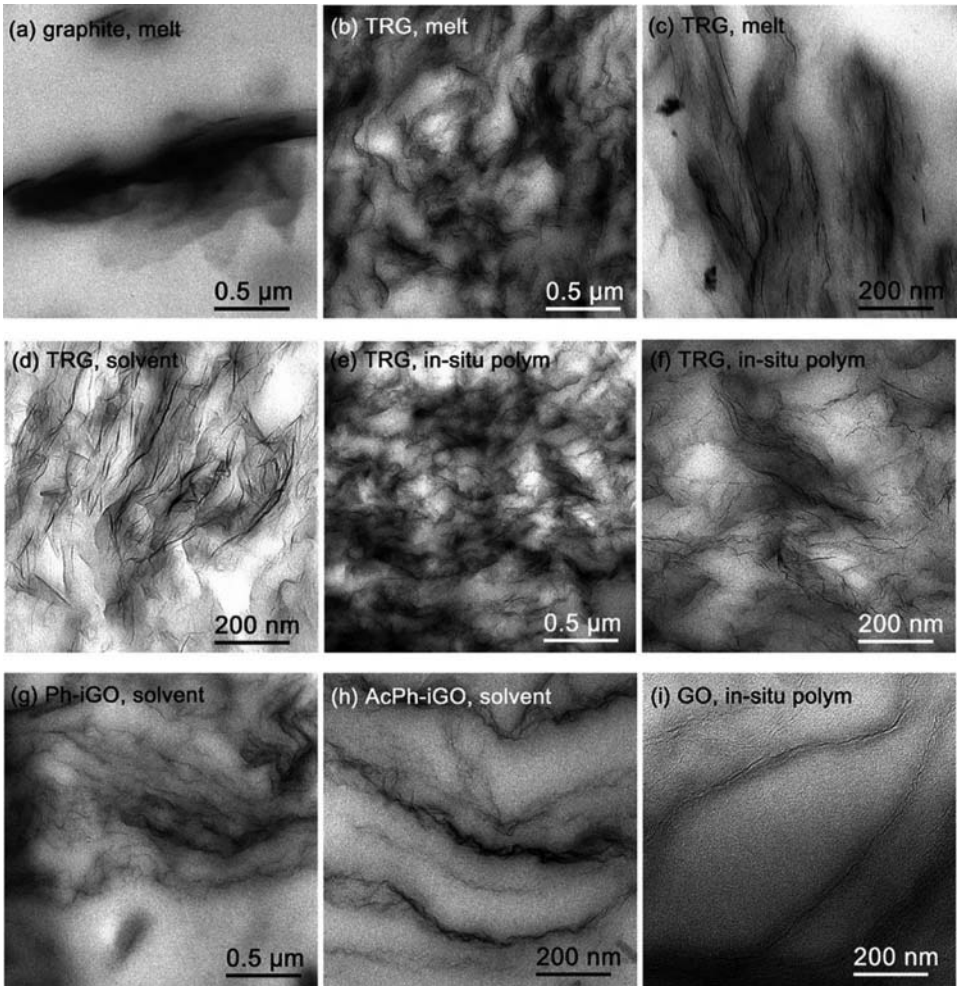

Figure 11. TEM micrographs of TPU composites filled with (a) 5 wt% (2.7 vol%) graphite, (b,c) 3 wt% (1.6 vol%) melt-processed TRG, (d) 3 wt% (1.6 vol%) solution blended TRG, (e,f) 3 wt% (1.6 vol%) *in situ* polymerized TRG, (g) 3 wt% (1.6 vol%) phenyl isocyanate-modified GO, (h) 3 wt% (1.6 vol%) acetyl phenyl isocyanate-modified GO, and (i) 2.8 wt% (1.5 vol%) *in situ* polymerized GO. Reproduced with permission from[129] Copyright 2010, American chemical society.

enhance barrier properties of the composites. Such large decreases in permeability are not widely reported in the literature for elastomer-based composites but it illustrates anyhow a tendency. However, surprisingly, homogenous dispersion of the filler in the matrix does not always lead to the best performance in permeation. Indeed, Yan et al.[131] have reported that a specifically segregated morphology obtained by the latex compounding method (LCM) could lead to improved barrier efficiency as compared to homogeneously dispersed and aligned platelets. Thus, Yan et al.[131] prepared natural rubber composites containing 4 phr of rGO through a latex co-coagulation method. Some samples were obtained directly from compression molding the coagulated material while others were homogenized on a two-roll mill prior to compression molding. Figure 12 shows the morphologies obtained with the two compounding methods.

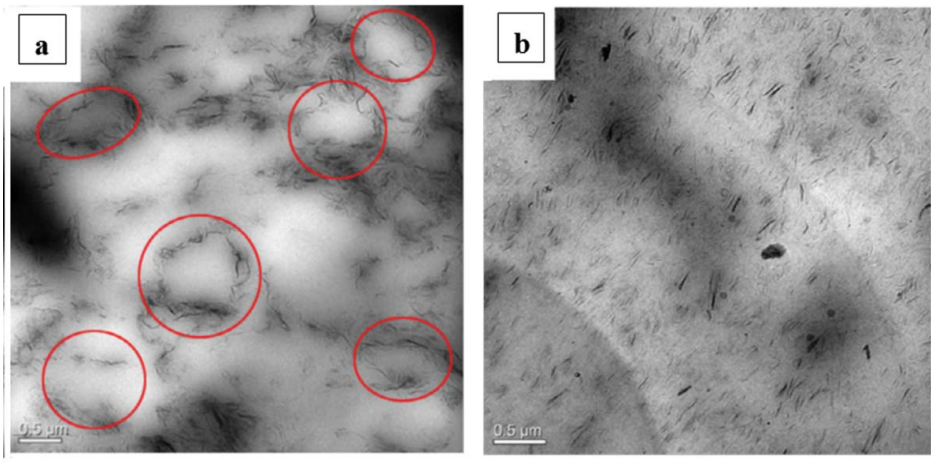

Figure 12. Composites containing 4 phr of rGO in natural rubber (NR) matrix prepared through two methods: (a) latex compounding and (b) homogenization in a two-roll mill. Adapted from[131].

While Fig. 12a shows a segregated morphology, with the graphene-based nanosheets being localized at the interfaces between latex particles, Fig. 12b displays a more homogenous dispersion in the elastomer matrix. Oxygen permeability of the these composites was also investigated (Fig. 13).

Both morphologies exhibited improved barrier properties of the composites in comparison with pristine NR but samples with a segregated structure showed greater permeability reduction as compared to homogenized samples (70% toward 30% at 4 phr loading). These results indicate that the connected network formed by rGO platelets is more efficient in diverting the permeant path than homogeneously dispersed platelets. The segregated morphology ensures a smaller inter-particle distance than homogenous distribution, thus creating barrier zones able to divert and slow down the permeant diffusion to a greater extent. Optimum dispersion for improvement of barrier properties is thus very dependent

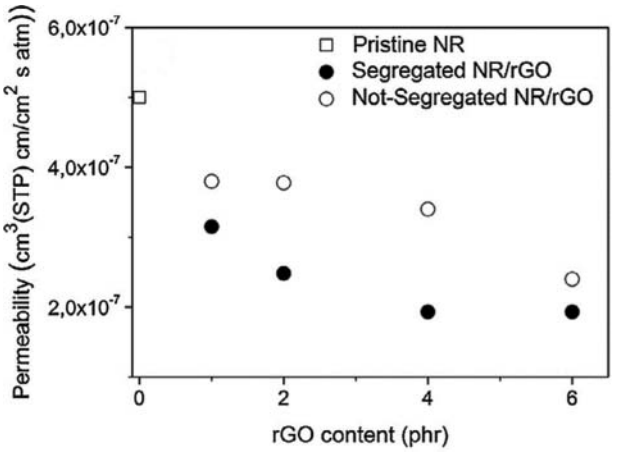

Figure 13. Oxygen permeability of NR-rGO composites as a function of rGO loading for the two types of morphologies. Adapted from[131].

on processing conditions. Other impermeable fillers with appropriate platelet morphology such as clays have also been used to increase barrier properties of polymers. However, graphene-based nanofillers were shown to perform better in reducing, *e.g.*, oxygen permeability than clays at same concentrations,[115] or to achieve same permeability reduction with remarkably lower loadings, approximately 50–70 times less.[116] Similarly, 0.001 wt% of graphene oxide was reported to provide equivalent improvement of water vapor barrier properties in polyimide as 8 wt% of montmorillonite, which was attributed to the much larger aspect ratio of GO platelets compared with the nanoclay.[117] Moreover, graphene and its derivatives have a significant advantage over clays as they can perform better in permeability reduction while preserving good mechanical properties of the composites and providing at the same time additional functional properties due to increased thermal and electrical conductivity.[3,119,137,144,145] Of course, as with nanofillers in general, graphene-based nanofillers can fulfill these expectations only if they are well dispersed in the polymer matrix.

3.2 Mechanical properties

Single-layer graphene has outstanding mechanical properties: it is stiff, flexible and displays a Young's modulus of 1 TPa and an ultimate strength of 130 GPa. On the contrary, rubber-based materials have low stiffness and break at relatively small stresses around 20 MPa. Due to this important contrast, many attempts have been made to reinforce rubbers through incorporation of GBMs in an elastomeric matrix.[7,119,146–148]

3.2.1 Tensile properties

Table 2 highlights the main results in tensile properties comparing the processing methods, the GBMs loadings and the elastomer matrix. Many reports have shown improvement of mechanical properties due to GBMs incorporation. Most studies deal with the incorporation of small content of GBMs into a polymeric matrix through direct or solution mixing. They mainly report an increase in Young's modulus and in tensile strength, and a decrease in elongation at break. However, these results appear to strongly depend upon the type of filler (lateral size, thickness, surface chemistry) and the mixing procedure.

3.2.1.1 Influence of filler size, shape, and aspect ratio. Different carbon-based fillers have been investigated by Schopp et al.[149] They prepared SBR composites containing 25 phr loading of, respectively, carbon black (CB), carbon nanotubes (CNTs), expanded graphite (EG), multilayer graphene (MLG, < 10 layers), chemically reduced graphite oxide (CRGO), and thermally reduced graphite oxide (TRGO). They used latex mixing followed by internal mixer and two-roll mill mixing. Stress–strain plots in Fig. 14 clearly indicate that TRGO and MLG lead to the most pronounced stiffening of the material with stress at 50% strain up to 14 times higher than pure SBR matrix.[149]

Tensile strength is also greatly increased (more than three times higher than neat SBR) but elongation at break is strongly impacted and is decreased by a factor 3. CRGO and CNTs lead to moderate increases in tensile strength ($\times$ 2) and stiffness ($\times$ 3) with a less pronounced loss in strain at break. CB and EG did not bring much changes compared to neat matrix properties, leading to a slight increase in stiffness and in tensile strength with no impact on elongation at break. The stiffening effect of these carbon-based fillers could be ranked the following way: TRGO>MLG>CRGO>CNTs>CB>EG. Hence, platelet-like

Table 2. Short literature review of data regarding the tensile properties of some GBMs/elastomer composites[a].

Filler	Loading	Matrix	Processing	Strain at break	Tensile strength	50% modulus	100% modulus	300% modulus	Reference
TRG	5 phr	NR latex	Pre-mixing in latex phase followed by two-roll mill	950% (× 1.1 as compared to neat NR)	6 MPa (× 1.5 as compared to neat NR)		1 MPa (× 2 as compared to neat NR)	5 MPa (× 6 as compared to neat NR)	147
TRG	5 phr	NR latex	two-roll mill	600% (/ 1.5)	11 MPa (× 2.8)		0.5 MPa (× 1)	1 MPa (× 1.25)	147
Chemically rGO	5 phr	NR latex	Pre-mixing in latex phase followed by two-roll mill	500% (/ 2)	9 MPa (× 2)		1 MPa (× 2)	4 MPa (× 4)	151
Chemically reduced GO	5 phr	NR latex	Pre-mixing in latex phase followed by solution mixing	< 100% (/ 8)	10 MPa (× 5)		—	—	151
Graphite	25 phr	SBR	Solution (THF), HAAKE and two-roll mill	66% (of the value obtained for the neat matrix)	148%	320%			178
TRG	25 phr	SBR	Solution (THF), HAAKE and two-roll mill	37%	991%	1520%			178
TRG	25 phr	SBR	Latex mixing, internal mixer and two-roll mill	88% (/ 3.7)		17.5 MPa (× 3)	10.9 MPa (× 14)		145
Multilayer graphene (<10 layers)	25 phr	SBR	Latex mixing, internal mixer and two-roll mill	91% (/ 3.6)		9.9 MPa (× 2)	6.5 MPa (× 8)		150
EG	25 phr	SBR	Latex mixing, internal mixer and two-roll mill	334% (× 1)		4.6 MPa (× 1)	1.1 MPa (× 1.4)	4.2 MPa (/ 1.1)	150
GO-octadecylamine	4 wt%	TPU	Solution (THF)	850% (/ 1.1)	35 MPa (× 1.3)		4 MPa (× 1.6)	10 MPa (× 1.4)	179
GO-octadecylamine	10 wt%	TPU	Solution (THF)	600% (/ 1.6)	17 MPa (/ 1.6)		4 MPa (× 1.6)	7 MPa (× 2)	179
GO-octadecylamine	50 wt%	TPU	Solution (THF)	10% (/ 9.5)	9 MPa (/3)				179
rGO	2 phr	NR latex	Latex co-coagulation followed by twin-roll mill	550% (/ 1.6)	27 MPa (× 2.7)				123
rGO	2 phr	NR latex	Latex co-coagulation (segregated morphology of the composites)	600% (/ 1.5)	18 MPa (× 1.8)				123
GO	0.3 wt%	LSR	*In situ* polymerization	40% (/ 1.3)	1.5 MPa (× 1.8)				148

(*Continued on next page*)

Table 2. (*Continued*)

Filler	Loading	Matrix	Processing	Strain at break	Tensile strength	50% modulus	100% modulus	300% modulus	Reference
EG	10 phr	NBR latex	Internal mixer	610% (× 1.5)	5.8 MPa (× 1.5)		1.8 MPa (× 1.6)		125
EG	10 phr	NBR latex	Latex compounding method followed by internal mixer	110% (/ 3.7)	11.8 MPa (× 3)		11.5 MPa (× 10.5)		125
rGO	2 wt%	NR latex	Ultrasonically-assisted latex mixing and two-roll mill	564% (/ 1.1)	25.2 MPa (× 1.5)		1.7 MPa (× 1.7)	6.6 MPa (× 2.8)	180
rGO	2 wt%	NR latex	Two-roll mill	600% (× 1)	18.8 MPa (× 1.1)		0.99 MPa (× 1)	2.47 MPa (× 1)	180
EG	10 phr	NBR latex	two-roll mill	260% (/ 1.2)	6.5 MPa (× 1.2)		2.5 MPa (× 1.7)		150

[a]Acronyms used: TRG (thermally reduced graphite oxide); EG (expanded graphite); rGO (reduced graphite oxide); GO (graphite oxide); NR (natural rubber); NBR (acrylonitrile-butadiene rubber); TPU (thermoplastic polyurethane); LSR (liquid silicone rubber).

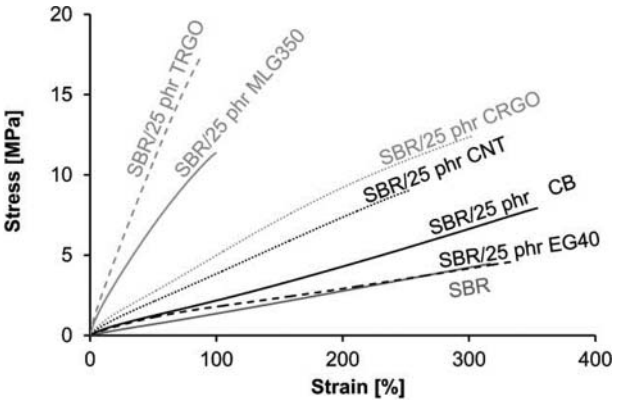

Figure 14. Stress–strain curves of carbon-based fillers/SBR composites at 25 phr. Reproduced with permission from[149] Copyright 2014, Wiley.

carbon fillers with small thickness exhibited the highest reinforcing effect on the SBR matrix. However, a strong reduction in strain at break is usually not desirable and CRGO filler might be more satisfactory for most common rubber applications where ability to withstand large deformations is required. Another feature, not investigated in this study, is the influence of the filler over the crosslinking density of the elastomer. Hence, the filler may interact with the curing system and lead to differences in crosslinking densities of the final composites, thus affecting their mechanical properties.[150] Similarly, Mao et al.[151] compared the efficiency of CB as compared to GO and observed that around 13 vol% (~32 phr) of CB (N330) were necessary to reach the same tensile strength as SBR composites containing only 2 vol% of GO.[151] Similar results were reported by Ozbas et al.[122] who showed that 1 wt% of TRGO in NR lead to similar moduli values as composites containing as much as 16 wt% of CB. Thus, GBMs show promising results for reinforcement of elastomers at low loading.

3.2.1.2 Influence of processing. Mechanical properties of elastomer composites are very dependent upon many parameters linked to the process. As a matter of fact, filler dispersion is strongly impacted by the processing technique and is of significant influence over the behavior of the composite. Besides, the elastomeric matrix may undergo degradation such as molar mass reduction during mixing. Another key feature is the nature and the amount of crosslinks formed during the vulcanization process. However, the features of the vulcanized network in the composites (crosslinking density and nature of crosslinks) compared to the pristine matrix is seldom studied in the literature. The following section will thus focus on process parameters affecting filler dispersion without taking into account any modification of the crosslinked network in the presence of the filler. Potts et al.[152,156] investigated the preparation of TRGO/NR composites prepared either in bulk by two-roll mill mixing or from latex via a latex mixing phase preceding twin-roll mill mixing. They observed a slight decrease in modulus at 100% and 300% strain for bulk-compounded composites at 2 phr loading of TRGO as compared to neat NR. On the contrary, latex-compounded composites with 2 phr showed over 40% improvement in modulus at 100% strain, as compared to the NR matrix.[152] Moreover, it was observed by using both scanning electronic microscopy (SEM) and transmission electronic microscopy that the latex pre-mixing step improved the dispersion of rGO in NR, which improves the moduli of the corresponding composites.

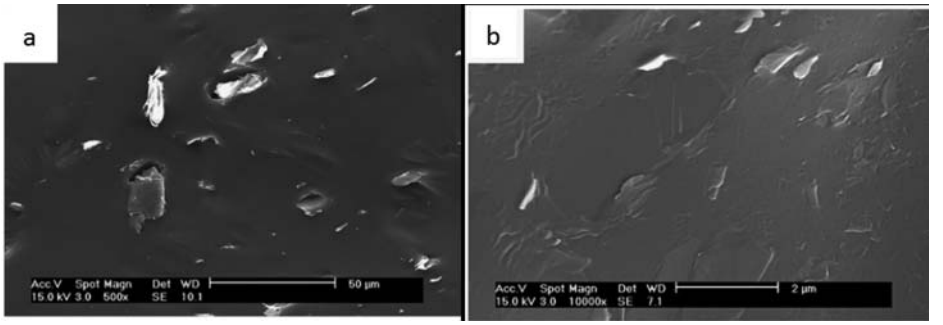

Figure 15. SEM images of EG/NBR composites with 5 phr of EG prepared with (a) direct blending and (b) latex compounding method. Adapted from[133].

Similarly, Yang et al.[133] observed better dispersion for EG/NBR composites prepared through latex compounding followed by internal mixing than for composites that underwent no latex precompounding phase. For example, Fig. 15 shows SEM pictures of EG/NBR composites with 5 phr loading of EG prepared either through direct bulk mixing or including a predispersion in latex phase.[123]

It can be seen clearly that EG-based aggregates are much smaller (from 25 μm to less than 1 μm) in the composite prepared through a latex premixing method. Moreover, tensile properties of EG/NBR composites prepared through latex mixing showed a significant increase of stresses even at 3 phr loading. The authors achieved a three times higher tensile strength at 10 phr loading than with unfilled NBR while they observed a strongly reduced elongation at break (110% *vs*. 410% for pure NBR).[133] The effect of latex compounding was further investigated by Yan et al.[131] Indeed, they dispersed rGO in NR latex using a latex co-coagulation method with or without further homogenization on a twin-roll mill. As discussed before, they showed that samples prepared through a one-step latex mixing exhibited a segregated morphology (Fig. 12) and performed better in permeability measurements. Figure 16 shows stress–strain curves of pure NR and composites with 2 phr loading of rGO with a segregated (not homogenized) or homogenous dispersion.

In Fig. 16, it can be observed that samples prepared through a one-step latex mixing ("not homogenized") exhibit higher modulus at both 100% and 300% elongation, higher tensile

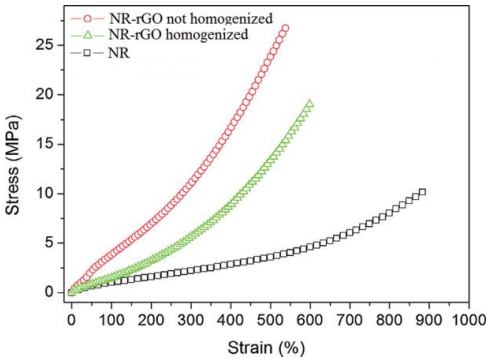

Figure 16. Stress–strain curves of pure NR and of rGO/NR composites with 2 phr loading of rGO, homogenized or not. Reproduced with permission from[131] Copyright 2014, Elsevier.

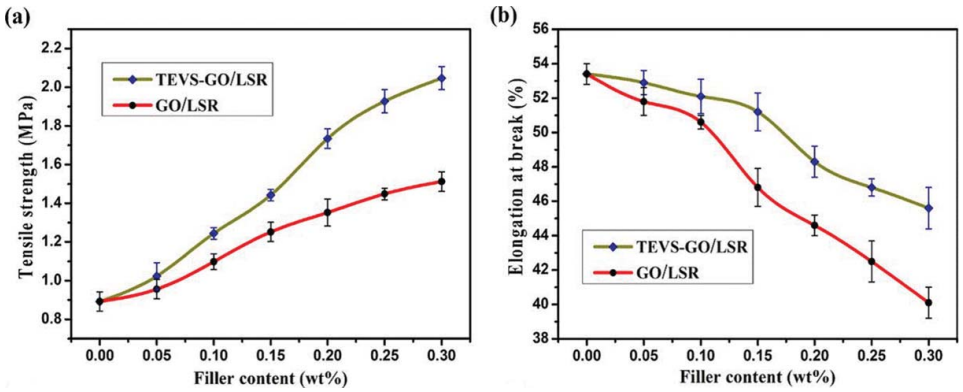

Figure 17. Mechanical properties of LSR-based composites (a) tensile strength and (b) elongation at break. Adapted from.[153]

strength (27 MPa *vs.* 19 MPa for homogenized samples) as well as a small decrease in elongation at break. These improved performances for segregated composites may be related to the formation of a stronger rGO network.[131]

3.2.1.3 Influence of graphene-based platelets functionalization. Influence of graphene-based platelets functionalization over mechanical properties was investigated by Zhao et al.[153] First, they functionalized GO using triethoxyvinylsilane (TEVS) followed by a *in situ* polymerization of liquid silicone rubber (LSR) in presence of TEVS-grafted GO. They also prepared un-functionalized composites with the same method and investigated mechanical properties of the composites at different filler contents. Figure 17 shows the tensile properties of the corresponding LSR-based composites.

Composites containing 0.3 wt% of functionalized GO showed slightly greater tensile strength (2 MPa *vs.* 1.5 MPa) as well as comparable strain at break (46% *vs.* 40%). These changes are anyhow very small and the functionalization did not bring significant enhancement in tensile properties of LSR composites.

Wang et al.[154] also investigated the effect of GO functionalization on tensile properties. They grafted octadecylamine onto GO and prepared SBR-based composites through melt compounding, with the filler being incorporated as a "paste" with ethanol, and by ensuring subsequent evaporation of the solvent during mixing on a twin-roll mill. Figure 18 shows stress–strain curves of SBR-based composites containing 3 wt% of modified and neat GO.

The composites containing the modified fillers exhibited higher tensile strength but lower stiffness than pristine GO. Both fillers led to increases in tensile strength, stresses at 100% and 300% elongation as well as strain at break compared to the pure SBR matrix. In this study, functionalization did not bring much improvement in tensile properties of the composites at low loading (3 phr). Thus, functionalization can be a means to improve filler dispersion but does not always lead to improved mechanical properties. Intrinsic filler parameters such as size, shape, and aspect ratio have shown to be of greater influence over properties of the composites.

3.2.2 Viscoelastic properties

Studying viscoelastic properties of the composites by dynamic mechanical analysis (DMA) provides information regarding molecular mobility of the polymer chains and about the

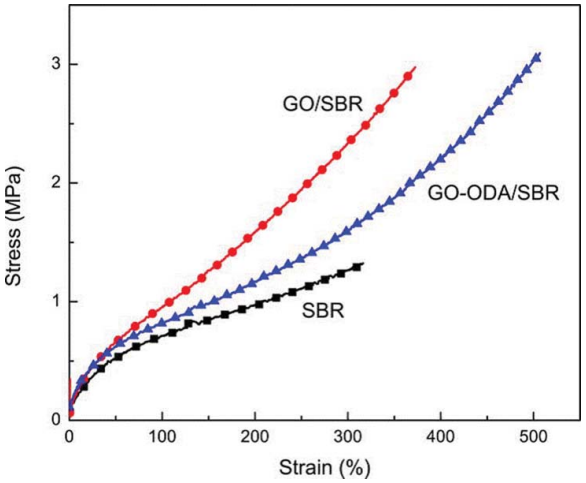

Figure 18. Stress–strain curves of pure SBR, GO/SBR, and GO-ODA/SBR composites at 3 phr loading. Reproduced with permission from[154] Copyright 2016, Wiley.

composite structure. The α relaxation temperature, $T\alpha$, associated with the glass transition temperature is obtained from tanδ maximum in a temperature sweep. It is related to molecular mobility which may be affected by strong interactions between elastomer chains and fillers. Reinforcement of the matrix due to filler incorporation can be observed through an increase in the storage modulus. Figure 19 shows a typical example of the evolutions of the storage modulus and tanδ with temperature for EG/NBR composites.[155] The samples referred to as "micro-composites" are prepared through simple twin-roll mill mixing while "nanocomposites" are prepared with previous latex mixing dispersion stage. These names refer to the final size of the particles in the composites, which result from the efficiency of the mixing process.

The measurements were recorded under a tension mode at a frequency of 1 Hz with a strain amplitude of 0.1% in the temperature range from $-50°C$ to $+ 80°C$. The heating rate was 3°C/min.

From Fig. 19a, an increase in the storage modulus (E') in the rubbery state (above $T\alpha$) can be observed for all composites due to some reinforcing effect which is more pronounced for "nanocomposites" that underwent a latex pre-dispersion step, than for "micro-composites" that were prepared through direct twin-roll mill mixing. Due to poor dispersion and distribution, "micro-composites" exhibit a very weak reinforcement, whereas the increase of E' for "nanocomposites" can be attributed to a better dispersion state.[156,157] Elastomer-filler and filler-filler interactions ("filler networks") lead to a significant increase in E'. Besides, the effect of the filler loading can be observed. The increase in filler loading from 5 phr to 10 phr leads to doubling the storage modulus at 60°C (from 1×10^7 Pa to 2×10^7 Pa). On Fig. 19b, the loss factor (tanδ) is represented as a function of temperature. Upon incorporation of EG, no effect is observed for "micro-composites" as compared to neat NBR, while a broadening and a decrease in tanδ peaks after $T\alpha$ is observed for "nanocomposites." According to the authors, the decreased volume fraction of elastomer in these "nanocomposites" associated with filler–matrix interactions are responsible for more heterogenous behavior of NBR molecules (broadening) and a decrease of intramolecular hysteresis in the $T\alpha$ region. The authors

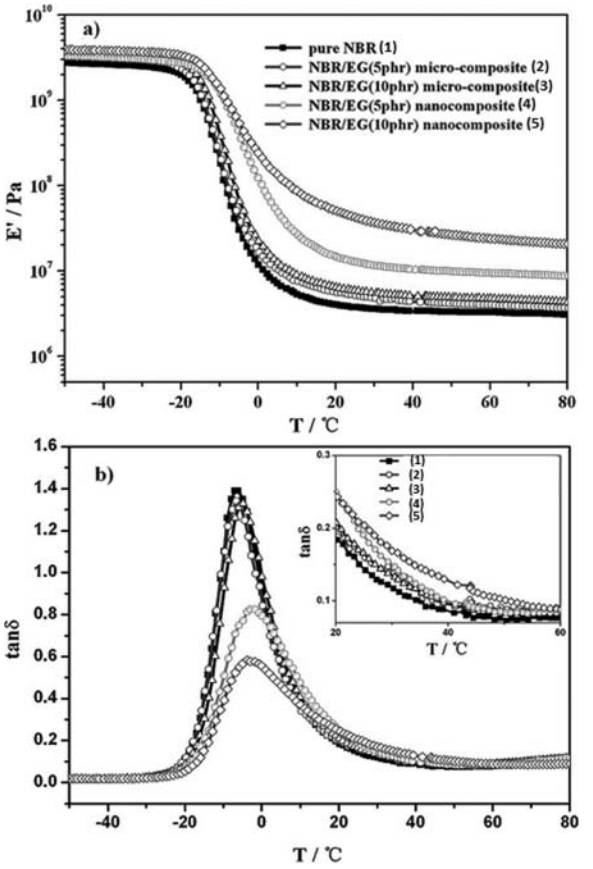

Figure 19. (a) Storage modulus of EG/NBR composites containing 5 phr and 10 phr of EG and (b) tanδ values. Reproduced with permission from[155] Copyright 2012, Elsevier.

point out a slight increase of tanδ beyond $T\alpha$, which they attribute to enhanced hysteretic mechanisms (friction between polymer chains, filler–matrix, and filler–filler interactions) when the filler volume fraction increases. However, it can be noted that this effect is very small (inset of Fig. 19b).

The viscoelastic behavior of filled elastomers typically exhibit enhanced non-linearity, known as the Payne effect. It is characterized by a drop of the storage modulus and the occurrence of a maximum of the loss modulus when strain is increased. It occurs at low strain, whereas unfilled elastomers exhibit non-linearity at larger strains without any peak on the loss modulus plot. Hence, unfilled rubbers show a linear behavior up to quite large strains while the elastic modulus of a filled rubber decreases with strain. It can be explained by adsorption and desorption of polymer chains on the filler surface under mechanical solicitation, leading to network collapse.[158,159]

Wang et al.[154] studied the behavior of SBR composites containing octadecylamine (ODA)-modified GO. Figure 20 shows plots of the storage modulus as a function of strain amplitude for various GO-ODA contents.

In Fig. 20, it can be observed that all compounds exhibit linear viscoelastic behavior at low strain amplitude and non-linear viscoelastic behavior at high strain rates. At 1 phr and 2 phr

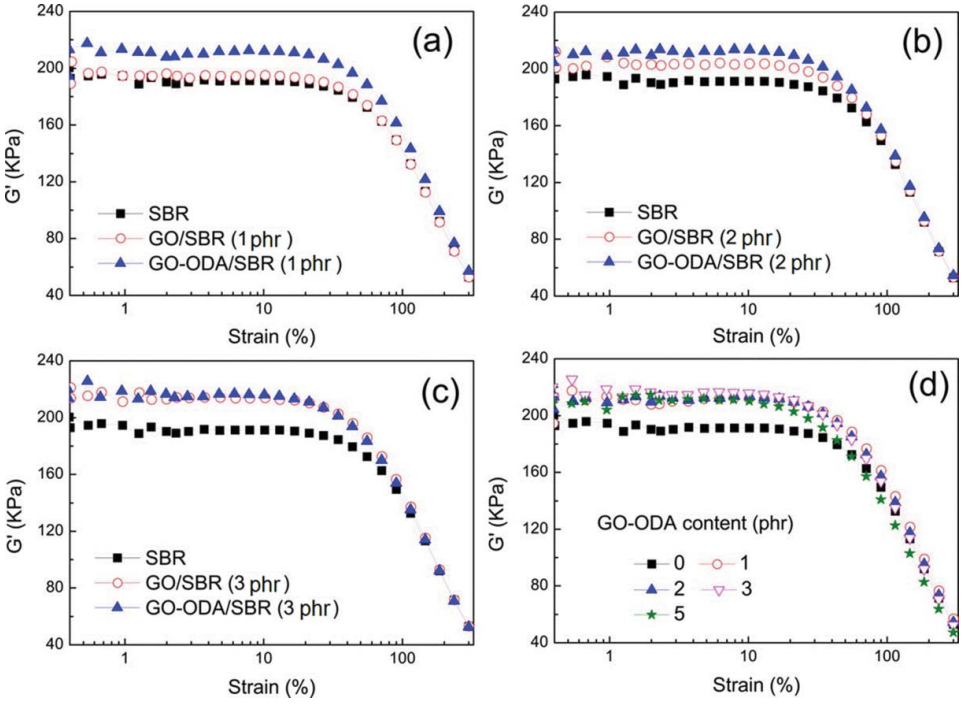

Figure 20. Storage modulus as a function of strain amplitude for crosslinked SBR-based composites with a filler content of (a) 1 phr, (b) 2 phr, (c) 3 phr, and (d) various GO-ODA content recorded at 1 Hz at 60°C. Reproduced with permission from[154] Copyright 2016, Wiley.

loadings, composites containing GO-ODA filler show slightly greater storage modulus than GO-filled samples suggesting a small reinforcement effect that may be attributed to a stronger interface due to ODA grafting onto GO.[154] Figure 20d shows that increased GO-ODA loading (5 phr) led to a narrower linear domain which can be attributed to the formation of a weak filler network which is more strain-sensitive. It can be pointed out though, that the influence of functionalization on viscoelastic properties of GO/SBR composites is very limited in this study. The numerous studies on graphene incorporation into elastomers to enhance mechanical properties reveal the strong potential of this nanofiller that might be used as a partial replacement of the very common CB filler in the future.

3.3 Thermal properties

3.3.1 Thermal stability

Graphene sheets are thermally stable up to more than 1,000°C and can thus increase the thermal stability of polymer composites. Nevertheless, most studies deal with the introduction of rGO, GNPs, or EG in elastomers, rather than single graphene sheets. Kim et al.[160] thus reported increased thermal stability of SBR/MLG composites at 1 wt% loading. In addition, some groups also observed an enhanced thermal stability for composites containing GO whereas GO is quite thermally unstable. Hence, Gan et al.[132] reported an increase of 44°C in the onset degradation temperature of liquid silicone rubber composites filled with 1 wt% loading of GO, as shown in Fig. 21.

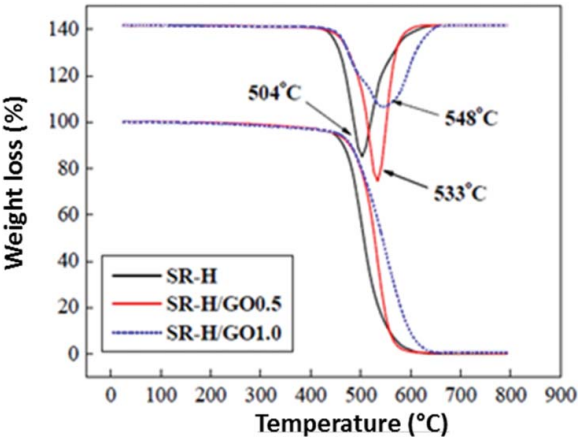

Figure 21. TGA data of silicone rubber (SR-H) composites filled with GO at 0.5 and 1 wt% . Adapted from.[132]

Therefore, incorporation of GBMs can be a good means to enhance thermal stability of elastomer composites.

3.3.2 Thermal conductivity

GBMs are very often reported to be efficient in increasing thermal conductivity of elastomers. A single graphene sheet displays a very high thermal conductivity and, if well dispersed in a matrix, it can lead to strong enhancements in thermal conductivities of rubbers. Its platelet morphology is moreover well adapted for thermal conduction, providing low interfacial resistance. Typical increase in thermal conductivity upon addition of GNPs is represented in Fig. 22 for SBR-based composites.

As shown in Fig. 22, an enhancement in thermal conductivity from 0.17 W/m.K for pristine SBR to 0.27 W/m.K upon addition of 5 vol% of GNPs was achieved by Araby et al.[161] They used a solution-blending technique followed by two-roll-mill mixing for the

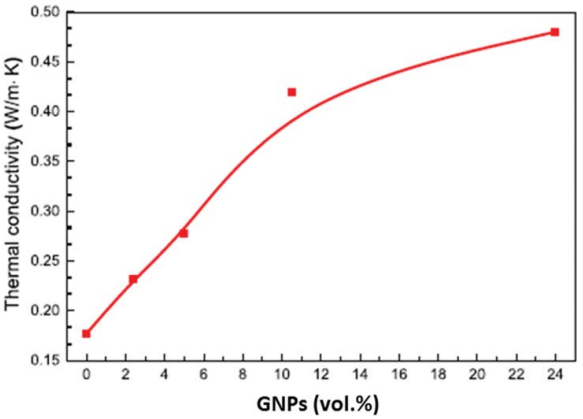

Figure 22. Thermal conductivity of SBR-based composites as a function of GNPs loading (using a thermal conductivity tester HC-110 according to ASTM C 518. The temperatures at the top and bottom molds were set at 50°C and 30°C with a sample size ø 51 mm . 6 mm). Adapted from.[161]

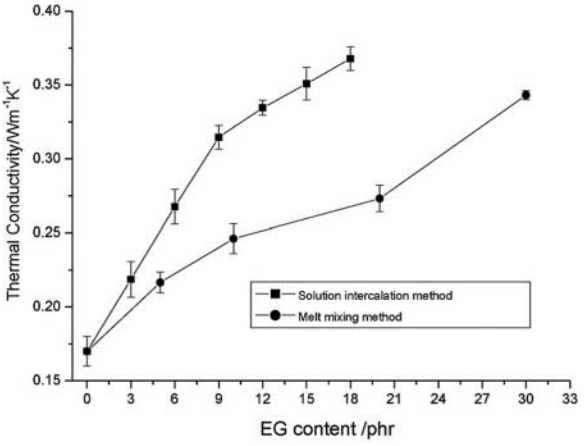

Figure 23. Thermal conductivity of EG/PDMS composites at various EG loadings. Reproduced with permission from[162] Copyright 2007, Elsevier.

preparation of the composites and a thermal conductivity as high as 0.48 W/m.K was reached at 24 vol% of GNPs content.[161] However, such a high loading of GNPs may strongly impact strain at break of the composites and will lead to high costs.

3.3.2.1 Influence of processing on thermal conductivity. Good contact between fillers is necessary for thermal conductivity enhancement. The final conductivity will thus depend on the dispersion quality, which results from filler geometry as well as the mixing process. To investigate the latter, Mu et al.[162] dispersed EG in silicon rubber at various loadings according to two methods: solution blending and direct melt mixing. Figure 23 shows the increase in thermal conductivity of these silicon-based composites as a function of the filler content.

Pure silicon matrix exhibited a 0.17 W/m.K thermal conductivity that was increased to 0.24 W/m.K and 0.32 W/m.K for melt-processed and solution-processed samples, respectively, at 9 phr loading. The authors observed enhanced thermal conductivities for all composites compared to the pristine silicon matrix, with a greater effect for solution-blended samples which exhibited better dispersion. They reported that the EG network was disrupted in the melt-blended composites while the solution process preserved the graphite network structure. By this method, more exfoliation and intercalation of elastomer chains between graphene layers can be achieved.[162] The authors suggested a structural interpretation for the origin of the higher thermal conductivity of solution-processed samples, as shown in Fig. 24.

Figure 24a represents large EG particles whose shapes and dimensions were not affected by the solution mixing. However, Fig. 24b shows particles that are much smaller and whose shape changed drastically under shear during melt mixing. The surface-to-volume ratio is then largely reduced and so higher loadings are necessary to achieve elevated thermal conductivity compared to solution-processed samples, in which the EG particles possess a higher aspect ratio.[162]

3.3.2.2 Influence of functionalization on thermal conductivity. Phonons are known to be responsible for the heat conduction in materials and to maximize their action, scattering

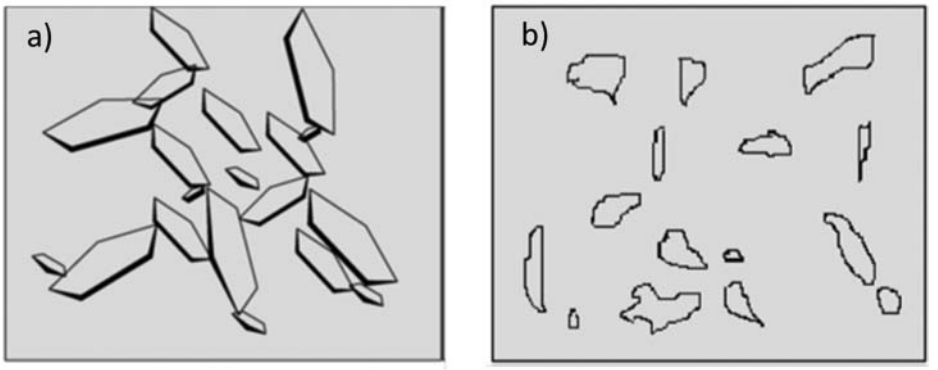

Figure 24. Schematic morphologies of EG/silicon composites prepared by (a) solution-processing and (b) melt-processing. Reproduced with permission from[162] Copyright 2007, Elsevier.

should be minimized. One method is to modify the graphene-based fillers by covalent coupling to the matrix to enhance filler–matrix interactions. Zhao et al.[153] introduced pristine and modified GO in liquid silicon rubber and observed that thermal conductivity was enhanced from 0.19 (pristine elastomer) to up to 0.38 W/m.K upon addition of modified GO at 0.3 wt% loading. Figure 25 shows the increase in thermal conductivity as a function of the filler content.

Both fillers increase thermal conductivity but the effect is more pronounced for TEVS-modified GO. A relative enhancement of up to 42% for TEVS-GO as compared to pristine GO/LSR composites was calculated at around 30 wt% loading. GBMs have thus proven to be effective in enhancing thermal stability and conductivity of elastomeric matrices. However, the increase in thermal conductivity is often limited by high interfacial thermal resistance between nanosheets and rubber. This phenomenon is known as Kapitza resistance[163,164] and is due to poor thermal coupling between GNPs and the elastomeric matrix.[162] Functionalization can thus be a means to improve this coupling by favoring the interfacial interaction between the graphitic filler and the elastomeric matrix.

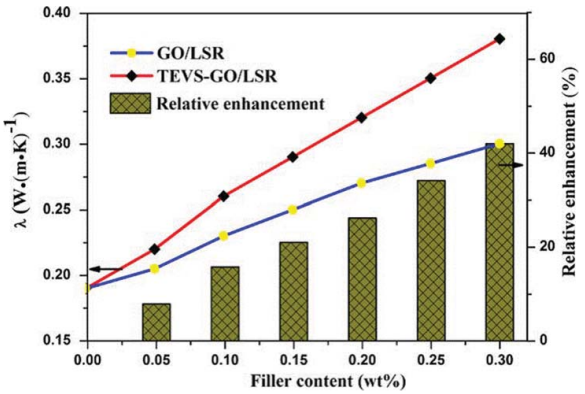

Figure 25. Thermal conductivity of silicon rubber (LSR) composites containing GO and TEVS-GO. Reproduced with permission from[153] Copyright 2015, Wiley.

Table 3. Short literature review of electrical properties of graphene-rubber composites.

Filler	Loading	Matrix	Process	Percolation threshold	Electrical resistivity	Electrical conductivity	Reference
GNPs	17 vol%	SBR	Solution and twin-roll mill	5 vol%	5.10^6 Ω / cm		156
GNPs	25 vol%	SBR	Twin-roll mill	16.5 vol%	10^{17} Ω / cm		165
Graphite	13 vol%	TPU	melt	3 vol%	10^6 Ω / cm		119
TRG	2.2 vol%	TPU	melt	0.25 vol%	10^3 Ω / cm		119
TRG	1.5 vol%	TPU	*In situ* polymerization	0.25 vol%	10^3 Ω / cm		119
TRG	1.7 vol%	TPU	solution	< 0.1 vol%	10^2 Ω / cm		119
rGO	1.78 vol%	NR	Latex mixing	0.62 vol%		0.03 Ω / cm	162
rGO	5 vol%	NR	Latex mixing and twin-roll milling	4.62 vol%		0.04 Ω / cm	162

3.4 Electrical properties

Table 3 highlights the main results in electrical properties comparing the processing methods, the GBMs loadings, and the elastomer matrix.

Elastomers are electrically insulating and the addition of conductive fillers (CB, carbon fibers, CNTs, GBMs…) can make them electrically conductive. This electrical conductivity is dependent on the filler electrical properties, its loading, size, and dispersion state in the host matrix. CB is commonly used to achieve electrical conductivity in elastomers. However, high loadings are usually necessary, impacting some other properties of the material, as failure properties. Carbon-based nanofillers are promising alternatives to carbon blacks in this application since their intrinsic electrical properties are some orders of magnitude higher, which offer the possibility to produce conductive elastomers at much lower filler loading.[165] CNTs have been reported to be very efficient in increasing electrical conductivity of polymers at a very low content (less than 1 vol%) so that GBMs also appear to be very promising for this application.

3.4.1 Electrical percolation concept

A major challenge when dealing with electrical conductivity is to ensure the creation of a conducting path inside the material. When filler loading is substantially low, the average distance between filler particles is greater than their size range and the fillers form individual particles rather than a conducting network. When a critical loading is reached, conduction can take place by a tunneling effect through the polymer layers surrounding the filler and electrical conductivity increases quickly. This critical concentration is called "percolation threshold."[166] It depends upon the filler content, size, morphology, and the state of dispersion and distribution in the material. The "ideal" dispersion of the filler in the matrix to increase electrical conductivity might not be the uniform dispersion needed for good mechanical properties, but rather a partial segregation that would create conductive paths. Close wrapping of the matrix on fillers would act negatively on electrical conductivity.[119] Araby et al.[161] investigated electrical properties of SBR filled with GNPs. They measured the electrical volume resistivity of these composites and observed a slight decrease below 5 vol% and a pronounced drop from 5 to 7 vol% (Fig. 26).

They interpreted these results using percolation theory. At low volume fraction, fillers cannot connect with each other and at a critical concentration (about 5 vol% in this study), the filler volume fraction is high enough to enable formation of conductive paths and so, to rapidly decrease electrical volume resistivity.

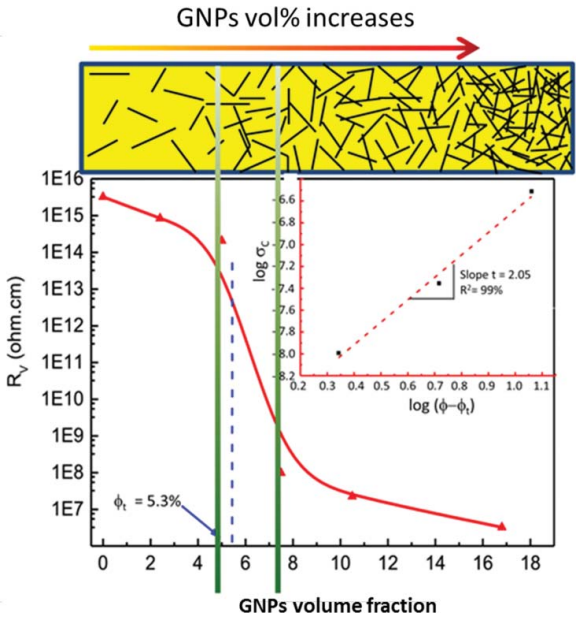

Figure 26. Electrical volume resistivity of SBR composites as a function of GNPs volume fraction. Adapted from.[161]

3.4.2 Influence of processing on electrical conductivity

The effect of processing on electrical surface resistance of composites filled with TRG flakes has been studied and the results are reported in Fig. 27.[129]

It appears that solution-blending is the most effective process in reaching low percolation threshold, with a value lower than 0.1 vol%. *In situ* polymerized and melt-compounded samples show a similar percolation threshold of 0.25 vol% but the former show a faster decrease in electrical surface resistance at higher loadings. The lowest resistance value (of around 10^2 Ω) was reached for TRG/TPU composites prepared from solution blending at around 1.7

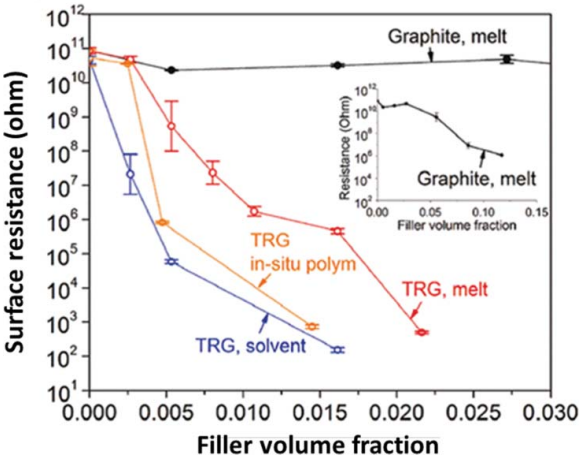

Figure 27. Surface resistance of GBMs/TPU composites prepared through different methods. Reproduced with permission from[129] Copyright 2010, American chemical society.

vol%. Another interesting feature in this work is the influence of filler size and specific surface area on the electrical properties. Graphite used in this study has a specific surface area of 29 m^2/g while TRG has a much higher specific surface area of 800 m^2/g. Graphite/TPU composites prepared through melt mixing showed a decrease in electrical surface resistance of about 5 orders of magnitude at more than 10 vol% while TRG/TPU composites achieved values 8 orders of magnitude lower than the neat matrix at only 2.2 vol%. Despite these spectacular results, it can be mentioned that surface resistance measurements are very sensitive to surface defects of the samples, which can be caused by processing. Moreover, the surface of a sample may not be much representative of the bulk (except for thin films). Therefore, volume resistivity measurements would have been preferable to draw suitable conclusions on the influence of processing. Influence of processing conditions upon the electrical conductivity of rGO/NR latex composites has also been investigated by Zhan et al.[167] They prepared composites using several mixing procedures. Some samples were prepared through direct latex coagulation, others were further homogenized on a twin-roll mill and others were obtained through direct blending. The results from the electrical conductivity measurements are shown in Fig. 28.

From these experiments, it appears clearly that samples prepared by direct melt mixing (HM and TR) again did not significantly increase electrical conductivity even at 8 vol% content. However, samples combining a latex mixing step with a twin-roll mill homogenization showed an increase in electrical conductivity of about 6 orders of magnitude with a percolation threshold lower than 5 vol%. Besides, samples prepared by latex mixing only performed best with an increase of about 7 orders of magnitude as compared to direct blended composites. They also showed a very low percolation threshold of less than 1 vol%. TEM pictures presented in Fig. 29 help to understand this phenomenon.

Figure 29a shows samples prepared through latex assembly. Segregated morphology can be observed with rGO platelets being arranged in circular shapes at the periphery of the elastomer latex particles, forming a network. On the contrary, samples that have been homogenized in a twin-roll mill show rather homogenous dispersion with orientation of the fillers along the milling direction (Fig. 29b). The formation of a conductive path in the segregated

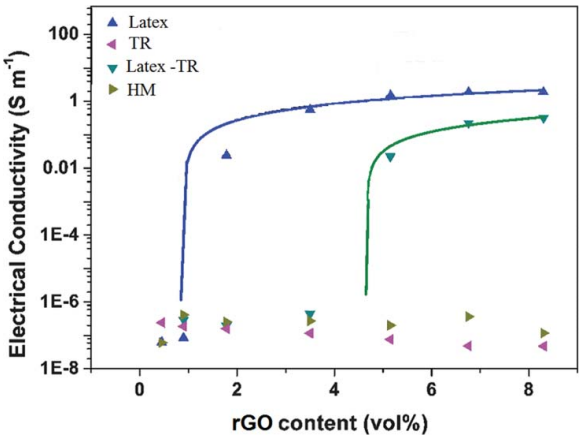

Figure 28. Electrical conductivity of rGO/NR composites prepared according to different methods. Latex: direct latex blending, TR: twin-roll mill mixing, Latex-TR: latex blending followed by twin-roll mill homogenization, and HM: HAAKE mixing. Adapted from.[167]

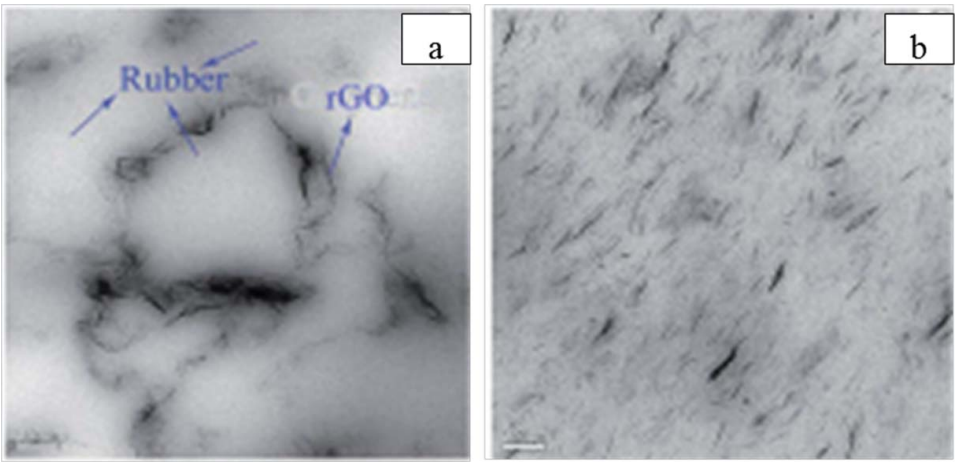

Figure 29. TEM images of rGO/NR composites prepared through (a) latex mixing and (b) latex assembly followed by twin-roll mixing. Adapted from.[167]

morphology is responsible for the higher electrical conductivity of the corresponding composites. Filler orientation also plays a significant role in reducing the percolation threshold and increasing electrical conductivity of the resulting material.[168–171] Higher electrical conductivities are achieved when fillers are interconnected. Random dispersion is thus often preferred to aligned platelets since there is a greater probability of platelets coming in contact with one another. Functionalization of the fillers may also be a means to increase electrical conductivity through improving dispersion and creating a stronger filler–matrix interface.[172] Combining different conductive fillers is also sometimes reported in the literature.[173] Outstanding electrical properties of graphene are thus of great interest in creating electrically conductive elastomer composites. Applications are numerous. Boland et al.,[174] for example, reported the use of graphene-rubber composites as strain sensors to monitor body motion.

3.4.3 Dielectric properties

Macromolecular dynamics can be studied through dielectric measurements. Hence, information on intermolecular motion as well as dipolar rotations can be evidenced from the dielectric relaxation spectrum. Most studies report an increase in dielectric permittivity of the composite upon addition of conductive fillers. Romasanta et al.[175] compared CNTs and rGO sheets in a PDMS matrix and observed a six-fold and ten-fold increase in the dielectric constant for reduced GO-based and CNTs-based composites, respectively. This difference may be due to the presence of some functional groups on rGO surface that reduce polarization process and thus improve the polymer–matrix interface. Several other groups performed dielectric studies on GBMs/rubber composites. Parameters affecting dielectric properties were found to be the loading, morphology, size, and dispersion state of the fillers, as for most of the properties of such composites.[176–181]

4. Summary and perspectives

Graphene is a promising nanomaterial that shows outstanding mechanical, thermal, electrical, and barrier properties. It is however hard to obtain perfect, defect-free graphene.

Methods such as chemical vapor deposition have proven to be efficient in growing single layers of high-quality graphene on very small surfaces, thus limiting its applications to nanoelectronics and lab-scale research. Other techniques such as oxidation/reduction of graphite-based fillers enable the production of much larger quantities of graphene-like sheets at lower costs. However, the latter materials usually present many defects like disruption of the conjugated π system, leading to inferior electrical properties. Such GBMs anyhow retain some interesting features of graphene such as relatively high mechanical and barrier properties and can thus be of great interest for use as fillers in polymers. Due to differences of several orders of magnitude in terms of mechanical, thermal, and electrical properties, significant effect of these nanofillers upon incorporation in polymeric materials such as elastomers can be expected. Several studies have shown the influence of the incorporation of GBMs in several elastomers on mechanical, thermal, electrical, and barrier properties of the composites. Several parameters affecting these enhancements were highlighted. Intrinsic characteristics of GBMs such as size, shape, and aspect ratio were proven to be of significant impact as well as processing conditions. Morphologies of the corresponding composites were observed to be affected by the process. Moreover, filler orientation was shown to be a key issue in permeability enhancement while the formation of a filler network inside the matrix was evidenced to be of major importance for electrical conductivity issues. In future, one challenge will be the production of inexpensive graphene-based composites at industrial scale from graphitic fillers which will require new processing techniques able to prepare stacks of graphene sheets with lower thicknesses and higher specific areas than the usual commercial graphitic fillers. In that frame, homogenous dispersion of GBMs in elastomers is also crucial for obtaining optimal thermal, electrical, and mechanical properties. Functionalization of graphene-based sheets was proven to be of significant interest to improve the filler dispersion and exfoliation in the matrix whereas they display inferior properties such as electrical conductivity. That is why other efforts should be made to exploit GBMs at nanoscale by creating a structural organization of graphene sheets ensuring lower percolation threshold.

References

1. Geim, A.; Novoselov, K. S. The Rise of Graphene. *Nature Materials*. **2007**, *6*, 183–191. doi:10.1038/nmat1849.
2. Kim, H.; Abdala, A. A.; Macosko, C. W. Graphene/Polymer Nanocomposites. *Macromolecules*. **2010**, *43*, 6515–6530. doi:10.1021/ma100572e.
3. Yoo, B. M.; Shin, H. J.; Yoon, H. W.; Park, H. B. Graphene and Graphene Oxide and their uses in Barrier Polymers: Review. *J. Appl. Polym. Sci.* **2014**, *131*, 39628. doi:10.1002/app.39628.
4. Wan, X.; Huang, Y.; Chen, Y. Focusing on Energy and Optoelectronic Applications: A Journey for graphene and graphene oxide at large scale. *Acc. Chem. Res.*. **2012**, *45*, 598–607. doi:10.1021/ar200229q.
5. Gu, W.; Zhang, W.; Li, X.; Zhu, H.; Wei, J.; Li, Z.; Shu, Q.; Wang, C.; Wang, K.; Shen, W.; Kang, F.; Wu, D. Graphene sheets from worm-like exfoliated graphite. *J. Mater. Chem.* **2009**, *19*, 3367–3369. doi:10.1039/b904093p.
6. Yang, J.; Tian, M.; Jia, Q.-X.; Zhang, L.-Q.; Li, X.-L. Influence of graphite particle size and shape on the properties of NBR. *J. Appl. Polym. Sci.* **2006**, *102*, 4007–4015. doi:10.1002/app.24844.
7. Sadasivuni, K. K.; Ponnamma, D.; Thomas, S.; Grohens, Y. Evolution from graphite to graphene elastomer composites. *Prog. Polym. Sci.* **2014**, *39*, 749–780. doi:10.1016/j.progpolymsci.2013.08.003.
8. Xiu-Yun, C. Graphene-like nanosheets synthesized by natural flaky graphite in Shandong, China. *Int. Nano Lett.* **2013**, *3*, 1–5. doi:10.1186/2228-5326-3-6.

9. Jacob George, J.; Bandyopadhyay, A.; Bhowmick, A. K. New Generation Layered Nanocomposites Derived from Ethylene-co-Vinyl acetate and Naturally Occurring Graphite. *J. Appl. Polym. Sci.* **2008**, *108*, 1603–1616. doi:10.1002/app.25067.
10. Sun, Y.; Yuan, L.; Liang, G.; Chang, J.; Gu, A. In situ Vacuum Exfoliation Plus Microwave Curing: A Facile and Green Technique for Preparing Polymeric Composites with very Good Dispersion Based on Expanded Graphite. *Polym. Compos.* **2015**, *36*, 385–388. doi:10.1002/pc.22953.
11. Zheng, W.; Wong, S.-C. Electrical Conductivity and Dielectric Properties of PMMA/Expanded Graphite Composites. *Compos. Sci. Technol.* **2003**, *63*, 225–235. doi:10.1016/S0266-3538(02)00201-4.
12. Ranjbar, B.; Mirzazadeh, H.; Katbab, A. A.; Hrymak, A. N. In situ Dynamic Vulcanization Process in Preparation of Electrically Conductive PP/EPDM Thermoplastic Vulcanizate/Expanded Graphite Nanocomposites: Effects of State of Cure. *J. Appl. Polym. Sci.* **2012**, *123*, 32–40. doi:10.1002/app.34414.
13. Bianco, A.; Cheng, H.-M.; Enoki, T.; Gogotsi, Y.; Hurt, R. H.; Koratkar, N.; Kyotani, T.; Monthioux, M.; Park, C. R.; Tascon, J. M.; Zhang, J. All in the Graphene Family–a recommended Nomenclature for Two-Dimensional Carbon Materials. *Carbon*. **2013**, *65*, 1–6. doi:10.1016/j.carbon.2013.08.038.
14. León, V.; Quintana, M.; Herrero, M. A.; Fierro, J. L. G.; Hoz, A.; de la Prato, M.; Vázquez, E. Few-layer Graphenes from Ball-Milling of Graphite with Melamine. *Chem. Commun.* **2011**, *47*, 10936–10938. doi:10.1039/c1cc14595a.
15. León, V.; Rodriguez, A. M.; Prieto, P.; Prato, M.; Vázquez, E. Exfoliation of Graphite with Triazine Derivatives under Ball-Milling Conditions: Preparation of Few-Layer Graphene via Selective Noncovalent Interactions. *ACS Nano*. **2014**, *8*, 563–571. doi:10.1021/nn405148t.
16. Ji, X.; Xu, Y.; Zhang, W.; Cui, L.; Liu, J. Review of Functionalization, Structure and Properties of Graphene/Polymer Composite Fibers. *Compos. Part Appl. Sci. Manuf.* **2016**, *87*, 29–45. doi:10.1016/j.compositesa.2016.04.011.
17. Georgakilas, V.; Tiwari, J. N.; Kemp, K. C.; Perman, J. A.; Bourlinos, A. B.; Kim, K. S.; Zboril, R. Noncovalent Functionalization of Graphene and Graphene Oxide for Energy Materials, Biosensing, Catalytic, and Biomedical Applications. *Chem. Rev.* **2016**, *116*, 5464–5519. doi:10.1021/acs.chemrev.5b00620.
18. Georgakilas, V.; Otyepka, M.; Bourlinos, A. B.; Chandra, V.; Kim, N.; Kemp, K. C.; Hobza, P.; Zboril, R.; Kim, K. S. Functionalization of graphene: Covalent and non-covalent approaches, derivatives and applications. *Chem. Rev.* **2012**, *112*, 6156–6214. doi:10.1021/cr3000412.
19. Tasis, D.; Tagmatarchis, N.; Bianco, A.; Prato, M. Chemistry of Carbon Nanotubes. *Chem. Rev.* **2006**, *106*, 1105–1136. doi:10.1021/cr050569o.
20. Karousis, N.; Tagmatarchis, N.; Tasis, D. Current Progress on the Chemical Modification of Carbon Nanotubes. *Chem. Rev.* **2010**, *110*, 5366–5397. doi:10.1021/cr100018g.
21. Liu, J.; Tang, J.; Gooding, J. J. Strategies for Chemical Modification of Graphene and Applications of Chemically Modified Graphene. *J. Mater. Chem.* **2012**, *22*, 12435–12452. doi:10.1039/c2jm31218b.
22. Voiry, D.; Vallés, C.; Roubeau, O.; Pénicaud, A. Dissolution and Alkylation of Industrially Produced Multi-Walled Carbon Nanotubes. *Carbon*. **2011**, *49*, 170–175. doi:10.1016/j.carbon.2010.08.057.
23. Layek, R. K.; Nandi, A. K. A Review on Synthesis and Properties of Polymer Functionalized Graphene. *Polymer*. **2013**, *54*, 5087–5103. doi:10.1016/j.polymer.2013.06.027.
24. Maity, N.; Mandal, A.; Nandi, A. K. Synergistic Interfacial Effect of Polymer Stabilized Graphene via non-Covalent Functionalization in Poly(Vinylidene Fluoride) Matrix Yielding Superior Mechanical and Electronic Properties. *Polymer*. **2016**, *88*, 79–93. doi:10.1016/j.polymer.2016.02.028.
25. Woszczyna, M.; Winter, A.; Grothe, M.; Willunat, A.; Wundrack, S.; Stosch, R.; Weimann, T.; Ahlers, F.; Turchanin, A. All-Carbon Vertical van derWaals Heterostructures: Non-destructive Functionalization of Graphene for Electronic Applications. *Adv. Mater.* **2014**, *26*, 4831–4837. doi:10.1002/adma.201400948.

26. Nottbohm, C. T.; Turchanin, A.; Beyer, A.; Stosch, R.; Gölzhäuser, A. Mechanically Stacked 1-nm-Thick Carbon Nanosheets: Ultrathin Layered Materials with Tunable Optical, Chemical, and Electrical Properties. *Small*. **2011**, *7*, 874–883. doi:10.1002/smll.201001993.
27. Luo, Z.; Somers, L. A.; Dan, Y.; Ly, T.; Kybert, N. J.; Mele, E. J.; Johnson, A. T. C. Size-Selective Nanoparticle Growth on Few-Layer Graphene Films. *Nano Lett*. **2010**, *10*, 777–781. doi:10.1021/nl9026605.
28. Zhong, X.; Jin, J.; Li, S.; Niu, Z.; Hu, W.; Li, R.; Ma, J. Aryne cycloaddition: highly efficient chemical modification of graphene. *Chem. Commun*. **2010**, *46*, 7340–7342. doi:10.1039/c0cc02389b.
29. Sun, Z.; Kohama, S.; Zhang, Z.; Lomeda, J. R.; Tour, J. M. Soluble Graphene Through Edge-Selective Functionalization. *Nano Res*. **2010**, *3*, 117–125. doi:10.1007/s12274-010-1016-2.
30. Sainsbury, T.; Passarelli, M.; Naftaly, M.; Gnaniah, S.; Spencer, S. J.; Pollard, A. J. Covalent Carbene Functionalization of Graphene: Toward Chemical Band-Gap Manipulation. *ACS Appl. Mater. Interfaces.* **2016**, *8*, 4870–4877. doi:10.1021/acsami.5b10525.
31. Sicinski, M.; Gozdek, T.; Bielinski, D. M.; Szymanowski, H.; Kleczewska, J.; Piatkowska, A. Plasma-Modified Graphene Nanoplatelets and Multiwalled Carbon Nanotubes as Fillers for Advanced Rubber Composites. *IOP Conf. Ser. Mater. Sci. Eng.* **2015**, *87*, 012012. doi:10.1088/1757-899X/87/1/012012.
32. Vadukumpully, S.; Gupta, J.; Zhang, Y.; Xu, G. Q.; Valiyaveettil, S. Functionalization of Surfactant Wrapped Graphenenanosheets with Alkylazides for Enhanced Dispersibility. *Nanoscale*. **2011**, *3*, 303–308. doi:10.1039/C0NR00547A.
33. Park, J.; Yan, M. Covalent Functionalization of Graphene with Reactive Intermediates. *Acc. Chem. Res.* **2013**, *46*, 181–189. doi:10.1021/ar300172h.
34. Prato, M.; Li, Q. C.; Wudl, F.; Lucchini, V. Addition of Azides to Fullerene C60: Synthesis of Azafulleroids. *J. Am. Chem. Soc.* **1993**, *115*, 1148–1150. doi:10.1021/ja00056a049.
35. Cases, M.; Duran, M.; Mestres, J.; Martín, N.; Solà, M. Mechanism of the Addition Reaction of Alkyl Azides to [60]Fullerene and the Subsequent N 2 Extrusion to Form Monoimino-[60]fullerenes. *J. Org. Chem.* **2001**, *66*, 433–442. doi:10.1021/jo0010431.
36. Han, J.; Gao, C. Functionalization of Carbon Nanotubes and Other Nanocarbons by Azide Chemistry. *Nano-Micro Lett*. **2010**, *2*, 213–226. doi:10.1007/BF03353643.
37. Gao, C.; He, H.; Zhou, L.; Zheng, X.; Zhang, Y. Scalable Functional Group Engineering of Carbon Nanotubes by Improved One-Step Nitrene Chemistry. *Chem. Mater.* **2009**, *21*, 360–370. doi:10.1021/cm802704c.
38. Tagmatarchis, N.; Prato, M. Functionalization of Carbon Nanotubes Via 1,3-Dipolar Cycloadditions. *J. Mater. Chem.* **2004**, *14*, 437–439. doi:10.1039/b314039c.
39. Choi, J.; Kim, K.; Kim, B.; Lee, H.; Kim, S. Covalent Functionalization of Epitaxial Graphene by Azidotrimethylsilane. *J. Phys. Chem. C.* **2009**, *113*, 9433–9435. doi:10.1021/jp9010444.
40. Strom, T. A.; Dillon, E. P.; Hamilton, C. E.; Barron, A. R. Nitrene Addition to Exfoliated Graphene: A one-Step Route to Highly Functionalized Graphene. *Chem. Commun.* **2010**, *46*, 4097–4099. doi:10.1039/c001488e.
41. Economopoulos, S. P.; Tagmatarchis, N. Chemical Functionalization of Exfoliated Graphene. *Chem. Eur. J.* **2013**, *19*, 12930–12936. doi:10.1002/chem.201302358.
42. Quintana, M.; Spyrou, K.; Grzelczak, M.; Browne, W. R.; Rudolf, P.; Prato, M. Functionalization of Graphene via 1,3-Dipolar Cycloaddition. *ACS Nano*. **2010**, *4*, 3527–3533. doi:10.1021/nn100883p.
43. Zhang, X.; Hou, L.; Cnossen, A.; Coleman, A. C.; Ivashenko, O.; Rudolf, P.; van Wees, B. J.; Browne, W. R.; Feringa, B. L. One-Pot Functionalization of Graphene with Porphyrin through Cycloaddition Reactions. *Chem. Eur. J.* **2011**, *17*, 8957–8964. doi:10.1002/chem.201100980.
44. Liu, H.; Ryu, S.; Chen, Z.; Steigerwald, M. L.; Nuckolls, C.; Brus, L. E. Photochemical Reactivity of Graphene. *J. Am. Chem. Soc.* **2009**, *131*, 17099–17101. doi:10.1021/ja9043906.
45. Chua, C. K.; Pumera, M. Covalent Chemistry on Graphene. *Chem. Soc. Rev.* **2013**, *42*, 3222–32233. doi:10.1039/c2cs35474h.
46. Voiry, D.; Roubeau, O.; Pénicaud, A. Stoichiometric Control of Single Walled Carbon Nanotubes Functionalization. *J. Mater. Chem.* **2010**, *20*, 4385–4391. doi:10.1039/c0jm00082e.

47. Lonkar, S. P.; Deshmukh, Y. S.; Abdala, A. A. Recent Advances in Chemical Modifications of Graphene. *Nano res*. **2015**, *8*, 1039–1074. doi:10.1007/s12274-014-0622-9.
48. Bottari, G.; Ángeles Herranz, A.; Wibmer, L.; Volland, M.; Rodríguez-Pérez, L.; Guldi, D. M.; as Hirsch, A.; Martín, N.; D'Souza, F.; Torres, T. Chemical Functionalization and Characterization of Graphene-Based Materials. *Chem. Soc. Rev.* **2017**, *46*, 4464–4500. doi:10.1039/C7CS00229G.
49. Parviz, D.; Das, S.; Ahmed, H. S. T.; Irin, F.; Bhattacharia, S.; Green, M. J. Dispersions of Non Covalently Functionalized Graphene with Minimal Stabilizer. *ACS Nano*. **2012**, *6*, 8857–8867. doi:10.1021/nn302784m.
50. Su, Q.; Pang, S. P.; Alijani, V.; Li, C.; Feng, X. L.; Mullen, K. Composites of Graphene with Large Aromatic Molecules. *Adv. Mater.* **2009**, *21*, 3191–3195. doi:10.1002/adma.200803808.
51. Liang, Y. Y.; Wu, D. Q.; Feng, X. L.; Mullen, K. Dispersion of Graphene Sheets in Organic Solvent Supported by Ionic Interactions. *Adv. Mater.* **2009**, *21*, 1679–1683. doi:10.1002/adma.200803160.
52. Pu, N. W.; Wang, C. A.; Liu, Y. M.; Sung, Y.; Wang, D. S.; Ger, M. D. Dispersion of Graphene in Aqueous Solutions with Different Types of Surfactants and the Production of Graphene Films by Spray or Drop Coating. *J. Taiwan Inst. Chem. E.* **2012**, *43*, 140–146. doi:10.1016/j.jtice.2011.06.012.
53. Fernandez-Merino, M. J.; Paredes, J. I.; Villar-Rodil, S.; Guardia, L.; Solis-Fernandez, P.; Salinas-Torres, D.; Cazorla-Amoros, D.; Morallon, E.; Martinez-Alonso, A.; Tascon, J. M. D. Investigating the Influence of Surfactants on the Stabilization of Aqueous Reduced Graphene Oxide Dispersions and the Characteristics of their Composite Films. *Carbon*. **2012**, *50*, 3184–3194. doi:10.1016/j.carbon.2011.10.039.
54. Hummers, W. S. Jr; Offeman, R. E. Preparation of Graphitic Oxide. *J. Am. Chem. Soc.* **1958**, *80*, 1339–1339. doi:10.1021/ja01539a017.
55. Dimiev, A. M.; Tour, J. M. Mechanism of Graphene Oxide Formation. *ACS Nano*. **2014**, *8*, 3060–3068. doi:10.1021/nn500606a.
56. Soldano, C.; Mahmood, A.; Dujardin, E. Production, Properties and Potential of Graphene. *Carbon*. **2010**, *48*, 2127–2150. doi:10.1016/j.carbon.2010.01.058.
57. Lerf, A.; He, H.; Forster, M.; Klinowski, J. Structure of Graphite Oxide Revisited. *J. Phys. Chem. B.* **1998**, *102*, 4477–4482. doi:10.1021/jp9731821.
58. He, H.; Riedl, T.; Lerf, A.; Klinowski, J. Solid-State Nmr Studies of the Structure of Graphite Oxide. *J. Phys. Chem.* **1996**, *100*, 19954–19958. doi:10.1021/jp961563t.
59. Szabo, T.; Berkesi, O.; Forgo, P.; Josepovits, K.; Sanakis, Y.; Petridis, D.; Dekany, I. Evolution of Surface Functional Groups in a Series of Progressively Oxidized Graphite Oxides. *Chem. Mater.* **2006**, *18*, 2740–2749. doi:10.1021/cm060258+.
60. Wang, G.; Wang, B.; Park, J.; Yang, J.; Shen, X.; Yao, J. Synthesis of Enhanced Hydrophilic and Hydrophobic Graphene Oxide Nanosheets by a Solvothermal Method. *Carbon*. **2009**, *47*, 68–72. doi:10.1016/j.carbon.2008.09.002.
61. Gudarzi, M. M.; Moghadam, M. H. M.; Sharif, F. Spontaneous Exfoliation of Graphite Oxide in Polar Aprotic Solvents as The Route to Produce Graphene Oxide – Organic Solvents Liquid Crystals. *Carbon*. **2013**, *64*, 403–415. doi:10.1016/j.carbon.2013.07.093.
62. Guo, F.; Kim, F.; Han, T. H.; Shenoy, V. B.; Huang, J.; Hurt, R. H. Hydration-Responsive Folding and Unfolding in Graphene Oxide Liquid Crystal Phases. *ACS Nano*. **2011**, *5*, 8019–8025. doi:10.1021/nn2025644.
63. Aboutalebi, S. H.; Jalili, R.; Esrafilzadeh, D.; Salari, M.; Gholamvand, Z.; Aminorroaya Yamini, S.; Konstantinov, K.; Shepherd, R. L.; Chen, J.; Moulton, S. E.; Innis, P. C.; Minett, A. I.; Razal, J. M.; Wallace, G. G. High-Performance Multifunctional Graphene Yarns: Toward Wearable All-Carbon Energy Storage Textiles. *ACS Nano*. **2014**, *8*, 2456–2466. doi:10.1021/nn406026z.
64. Kim, J. E.; Han, T. H.; Lee, S. H.; Kim, J. Y.; Ahn, C. W.; Yun, J. M.; Kim, S. O. Graphene Oxide Liquid Crystals. *Angew. Chem. Int. Ed.* **2011**, *50*, 3043–3047. doi:10.1002/anie.201004692.
65. Dan, B.; Behabtu, N.; Martinez, A.; Evans, J. S.; Kosynkin, D. V.; Tour, J. M.; Pasquali, M.; Smalyukh, I. I. Liquid Crystals of Aqueous, Giant Graphene Oxide Flakes. *Soft Matter*. **2011**, *7*, 111546–11159. doi:10.1039/c1sm06418e.
66. Lomeda, J. R.; Green, M. J.; Higginbotham, A. L.; Sinitskii, A.; Kosynkin, D.; Tsentalovitch, D.; Parra-Vasquez, G.; Schmidt, J.; Kesselman, E.; Cohen, Y.; Talmon, Y.; Tour, J. M.; Pasquali, M.

Spontaneous High-Concentration Dispersions and Liquid Crystals of Graphene. *Nat. Nanotechnol.* **2010**, *5*, 406–411. doi:10.1038/nnano.2010.86.
67. Paredes, J. I.; Villar-Rodil, S.; Martinez-Alonso, A.; Tascon, J. M. D. Graphene Oxide Dispersions in Organic Solvents. *Langmuir*. **2008**, *24*, 10560–10564. doi:10.1021/la801744a.
68. Dreyer, D. R.; Park, S.; Bielawski, C. W.; Ruoff, R. S. The Chemistry of Graphene Oxide. *Chem. Soc. Rev.* **2010**, *39*, 228–240. doi:10.1039/B917103G.
69. Szabó, T.; Tombácz, E.; Illés, E.; Dékány, I. Enhanced Acidity and Ph-Dependent Surface Charge Characterization of Successively Oxidized Graphite Oxides. *Carbon*. **2006**, *44*, 537–545. doi:10.1016/j.carbon.2005.08.005.
70. Li, D.; Müller, M. B.; Gilje, S.; Kaner, R. B.; Wallace, G. G. Processable Aqueous Dispersions of Graphene Nanosheets. *Nat. Nanotechnol.* **2009**, *3*, 101–105. doi:10.1038/nnano.2007.451.
71. Xu, Z.; Gao, C. Aqueous Liquid Crystals of Graphene Oxide. *ACS Nano*. **2011**, *5*, 2908–2915. doi:10.1021/nn200069w.
72. Ogino, I.; Yokoyama, Y.; Iwamura, S.; Mukai, S. R. Exfoliation of Graphite Oxide in Water Without Sonication: Bridging Length Scales from Nanosheets to Macroscopic Materials. *Chem. Mater.* **2014**, *26*, 3334–3339. doi:10.1021/cm501305c.
73. Gómez-Navarro, C.; Weitz, R. T.; Bittner, A. M.; Scolari, M.; Mews, A.; Burghard, M.; Kern, K. Electronic Transport Properties of Individual Chemically Reduced Graphene Oxide Sheets. *Nano Lett*. **2007**, *7*, 3499–3503. doi:10.1021/nl072090c.
74. Dikin, D. A.; Stankovich, S.; Zimney, E. J.; Piner, R. D.; Dommett, G. H. B.; Evmenenko, G.; Nguyen, S. T.; Ruoff, R. S. Preparation and Characterization of Graphene Oxide Paper. *Nature* **2007**, *448*, 457–460. doi:10.1038/nature06016.
75. Zhu, Y.; Murali, S.; Cai, W.; Li, X.; Suk, J. W.; Potts, J. R.; Ruoff, R. S. Graphene and Graphene Oxide: Synthesis, Properties, and Applications. *Adv. Mater.* **2010**, *22*, 3906–3924. doi:10.1002/adma.201001068.
76. Rourke, J. P.; Pandey, P. A.; Moore, J. J.; Bates, M.; Kinloch, I. A.; Young, R. J.; Wilson, N. R. The Real Graphene Oxide Revealed: Stripping the Oxidative Debris from the Graphene-like Sheets. *Angew. Chem. Int. Ed.* **2011**, *50*, 3173–3177. doi:10.1002/anie.201007520.
77. Chua, C. K.; Pumera, M. Chemical Reduction of Graphene Oxide: A Synthetic Chemistry Viewpoint. *Chem Soc Rev*. **2014**, *43*, 291–312. doi:10.1039/C3CS60303B.
78. Thomas, H. R.; Day, S. P.; Woodruff, W. E.; Vallés, C.; Young, R. J.; Kinloch, I. A.; Morley, G. W.; Hanna, J. V.; Wilson, N. R.; Rourke, J. P. Deoxygenation of Graphene Oxide: Reduction or Cleaning. *Chem. Mater.* **2013**, *25*, 3580–3588. doi:10.1021/cm401922e.
79. Park, S.; An, J.; Potts, J. R.; Velamakanni, A.; Murali, S.; Ruoff, R. S. Hydrazine-Reduction of Graphite- and Graphene Oxide. *Carbon*. **2011**, *49*, 3019–3023. doi:10.1016/j.carbon.2011.02.071.
80. Dreyer, D. R.; Murali, S.; Zhu, Y.; Ruoff, R. S.; Bielawski, C. W. Reduction of Graphite Oxide Using Alcohols. *J. Mater. Chem.* **2011**, *21*, 3443–3447. doi:10.1039/C0JM02704A.
81. Potts, J. R.; Dreyer, D. R.; Bielawski, C. W.; Ruoff, R. S. Graphene-Based Polymer Nanocomposites. *Polymer*. **2011**, *52*, 5–25. doi:10.1016/j.polymer.2010.11.042.
82. Park, S.; Ruoff, R. S. Chemical Methods for the Production of Graphenes. *Nat. Nanotechnol.* **2009**, *4*, 217–224. doi:10.1038/nnano.2009.58.
83. Thakur, S.; Karak, N. Alternative Methods and Nature-Based Reagents for the Reduction of Graphene Oxide: A Review. *Carbon*. **2015**, *94*, 224–242. doi:10.1016/j.carbon.2015.06.030.
84. Gao, J.; Liu, F.; Liu, Y.; Ma, N.; Wang, Z.; Zhang, X. Environment-Friendly Method To Produce Graphene That Employs Vitamin C and Amino Acid. *Chem. Mater.* **2010**, *22*, 2213–2218. doi:10.1021/cm902635j.
85. Zhang, J. L.; Yang, H. J.; Shen, G. X.; Cheng, P.; Zhang, J. Y.; Guo, S. W. Reduction of Graphene Oxide Via L -Ascorbic Acid. *Chem. Commun*. **2010**, *46*, 1112–1114. doi:10.1039/B917705A.
86. Fernández-Merino, M. J.; Guardia, L.; Paredes, J. I.; Villar-Rodil, S.; Solís-Fernández, P.; Martínez-Alonso, A.; Tascón, J. M. D. Vitamin C is an Ideal Substitute for Hydrazine in the Reduction of Graphene Oxide Suspensions. *J. Phys. Chem. C.* **2010**, *114*, 6426–6432. doi:10.1021/jp100603h.

87. Bose, S.; Kuila, T.; Mishra, A. K.; Kim, N. H.; Lee, J. H. Dual Role of Glycine as a Chemical Functionalizer and a Reducing Agent in the Preparation of Graphene: An Environmentally Friendly Method. *J. Mater. Chem*. **2012**, *22*, 9696–9703. doi:10.1039/c2jm00011c.
88. Tran, D. N. H.; Kabiri, S.; Losic, D. A Green Approach for the Reduction of Graphene Oxide Nanosheets Using Non-Aromatic Amino Acids. *Carbon*. **2014**, *76*, 193–202. doi:10.1016/j.carbon.2014.04.067.
89. Stankovich, S.; Dikin, D. A.; Piner, R. D.; Kohlhaas, K. A.; Kleinhammes, A.; Jia, Y.; Wu, Y.; Nguyen, S. T.; Ruoff, R. S. Synthesis of Graphene-Based Nanosheets Via Chemical Reduction of Exfoliated Graphite Oxide. *Carbon*. **2007**, *45*, 1558–1565. doi:10.1016/j.carbon.2007.02.034.
90. Stankovich, S.; Piner, R. D.; Chen, X.; Wu, N.; Nguyen, S. T.; Ruoff, R. S. Stable Aqueous Dispersions of Graphitic Nanoplatelets Via the Reduction Of Exfoliated Graphite Oxide in the Presence of Poly(Sodium 4-Styrenesulfonate). *J. Mater. Chem.* **2006**, *16*, 155–158. doi:10.1039/B512799H.
91. Lotya, M.; Hernandez, Y.; King, P. J.; Smith, R. J.; Nicolosi, V.; Karlsson, L. S.; Blighe, F. M.; De, S.; Wang, Z.; McGovern, I. T.; Duesberg, G. S.; Coleman, J. N. Liquid Phase Production of Graphene by Exfoliation of Graphite in Surfactant/Water Solutions. *J. Am. Chem. Soc.* **2009**, *131*, 3611–3620. doi:10.1021/ja807449u.
92. Cao, N.; Zhang, Y. Study of Reduced Graphene Oxide Preparation by Hummers' Method and Related Characterization. *J. Nanomater.* **2015**, *2015*, 1–5.
93. Khan, M.; Al-Marri, A. H.; Khan, M.; Mohri, N.; Adil, S. F.; Al-Warthan, A.; Siddiqui, M. R. H.; Alkhathlan, H. Z.; Berger, R.; Tremel, W.; Tahir, M. N. Pulicaria Glutinosa Plant Extract: A Green And Eco-Friendly Reducing Agent for the Preparation of Highly Reduced Graphene Oxide. *RSC Adv*. **2014**, *4*, 24119–24125. doi:10.1039/C4RA01296H.
94. Schniepp, H. C.; Li, J.-L.; McAllister, M. J.; Sai, H.; Herrera-Alonso, M.; Adamson, D. H.; Prud'homme, R. K.; Car, R.; Saville, D. A.; Aksay, I. A. Functionalized Single Graphene Sheets Derived from Splitting Graphite Oxide. *J. Phys. Chem. B*. **2006**, *110*, 8535–8539. doi:10.1021/jp060936f.
95. Bai, Y.; Cai, H.; Qiu, X.; Fang, X.; Zheng, J.: Effects of Graphene Reduction Degree on Thermal Oxidative Stability of Reduced Graphene Oxide/Silicone Rubber Nanocomposites. *High Perform. Polym*. **2015**, *27*, 997–1006. doi:10.1177/0954008315604205.
96. Stankovich, S.; Dikin, D. A.; Dommett, G. H. B.; Kohlhaas, K. M.; Zimney, E. J.; Stach, E. A.; Piner, R. D.; Nguyen, S. T.; Ruoff, R. S. Graphene-Based Composite Materials. *Nature*. **2006**, *442*, 282–286. doi:10.1038/nature04969.
97. Sharon, M.; Sharon, M. *Graphene: an introduction to the fundamentals and industrial applications*. Wiley: Hoboken, New Jersey, **2015**.
98. Wang, H.; Robinson, J. T.; Li, X.; Dai, H. Solvothermal Reduction of Chemically Exfoliated Graphene Sheets. *J. Am. Chem. Soc.* **2009**, *131*, 9910–9911. doi:10.1021/ja904251p.
99. Dubin, S.; Gilje, S.; Wang, K.; Tung, V. C.; Cha, K.; Hall, A. S.; Farrar, J.; Varshneya, R.; Yang, Y.; Kaner, R. B. A One-Step, Solvothermal Reduction Method for Producing Reduced Graphene Oxide Dispersions in Organic Solvents. *ACS Nano*. **2010**, *4*, 3845–3852. doi:10.1021/nn100511a.
100. Zhou, Y.; Bao, Q.; Tang, L. A. L.; Zhong, Y.; Loh, K. P. Hydrothermal Dehydration for the "Green" Reduction of Exfoliated Graphene Oxide to Graphene and Demonstration of Tunable Optical Limiting Properties. *Chem. Mater.* **2009**, *21*, 2950–2956. doi:10.1021/cm9006603.
101. Lin, Z.; Yao, Y.; Li, Z.; Liu, Y.; Li, Z.; Wong, C.-P. Solvent-Assisted Thermal Reduction of Graphite Oxide. *J. Phys. Chem. C.* **2010**, *114*, 14819–14825. doi:10.1021/jp1049843.
102. Chen, W.; Yan, L.; Bangal, P. R. Preparation of Graphene by the Rapid and Mild Thermal Reduction of Graphene Oxide Induced by Microwaves. *Carbon*. **2010**, *48*, 1146–1152. doi:10.1016/j.carbon.2009.11.037.
103. Zhu, Y.; Murali, S.; Stoller, M. D.; Velamakanni, A.; Piner, R. D.; Ruoff, R. S. Microwave Assisted Exfoliation and Reduction of Graphite Oxide for Ultracapacitors. *Carbon*. **2010**, *48*, 2118–2122. doi:10.1016/j.carbon.2010.02.001.
104. Hagstrom, S.; Lyon, H. B.; Somorjai, G. A. Surface Structures on the Clean Platinum (100) Surface. *Phys. Rev. Lett.* **1965**, *15*, 491–493. doi:10.1103/PhysRevLett.15.491.
105. De, S. K. ed: *Rubber technologist's handbook*. Rapra Technology Ltd: Shrewsbury, Shropshire, 2001.

106. Leblanc, J. L. Rubber–Filler Interactions and Rheological Properties in Filled Compounds. *Prog. Polym. Sci.* **2002**, *27*, 627–687. doi:10.1016/S0079-6700(01)00040-5.
107. Boehm, H. P. Some Aspects of the Surface Chemistry of Carbon Blacks and Other Carbons. *Carbon*. **1994**, *32*, 759–769. doi:10.1016/0008-6223(94)90031-0.
108. Papirer, E.; Dentzer, J.; Li, S.; Donnet, J. B. Surface Groups on Nitric Acid Oxidized Carbon Black Samples Determined By Chemical and Thermodesorption Analyses. *Carbon*. **1991**, *29*, 69–72. doi:10.1016/0008-6223(91)90096-2.
109. Donnet, J. B. Structure and Reactivity of Carbons: From Carbon Black to Carbon Composites. *Carbon*. **1982**, *20*, 267–282. doi:10.1016/0008-6223(82)90002-1.
110. Kuilla, T.; Bhadra, S.; Yao, D.; Kim, N. H.; Bose, S.; Lee, J. H. Recent Advances in Graphene Based Polymer Composites. *Prog. Polym. Sci.* **2010**, *35*, 1350–1375. doi:10.1016/j.progpolymsci.2010.07.005.
111. Ma, J.; Zhang, L.-Q.; Geng, L. Manufacturing Techniques of Rubber Nanocomposites. In: *Rubber nanocomposites*; Thomas, S., Stephen, R, Eds., pp. 21–62. Weiley & Sons: Chichester, UK, 2010.
112. Funt, J. M. Rubber Mixing. *Rubber Chem. Technol.* **1980**, *53*, 772–779. doi:10.5254/1.3535057.
113. Collin, V.; Boudimbou, I.; Peuvrel-Disdier, E. New Insights in Dispersion Mechanisms of Carbon Black in A Polymer Matrix Under Shear by Rheo-Optics. *J. Appl. Polym. Sci.* **2013**, *127*, 2121–2131. doi:10.1002/app.37769.
114. Collin, V.; Peuvrel-Disdier, E. Dispersion Mechanisms of Carbon Black in an Elastomer Matrix. *Elastomery*. **2005**, *9*, 9–15.
115. Sadasivuni, K. K.; Saiter, A.; Gautier, N.; Thomas, S.; Grohens, Y. Effect of Molecular Interactions on the Performance of Poly(Isobutylene-Co-Isoprene)/Graphene and Clay Nanocomposites. *Colloid. Polym. Sci*. **2013**, *291*, 1729–1740 doi:10.1007/s00396-013-2908-y.
116. Compton, O. C.; Kim, S.; Pierre, C.; Torkelson, J. M.; Nguyen, S. T. Crumpled Graphene Nanosheets as Highly Effective Barrier Property Enhancers. *Adv. Mater*. **2010**, *22*(42), 4759–4763 doi:10.1002/adma.201000960.
117. Tan, B.; Thomas, N. L. A Review of the Water Barrier Properties of Polymer/Clay and Polymer/Graphene Nanocomposites. *J. Membr. Sci.* **2016**, *514*, 595–612 doi:10.1016/j.memsci.2016.05.026.
118. Pavlidou, S.; Papaspyrides, C. A Review on Polymer–Layered Silicate Nanocomposites. *Prog. Polym. Sci.* **2008**, *33*, 1119–1198. doi:10.1016/j.progpolymsci.2008.07.008.
119. Papageorgiou, D. G.; Kinloch, I. A.; Young, R. J. Graphene/Elastomer Nanocomposites. *Carbon*. **2015**, *95*, 460–484. doi:10.1016/j.carbon.2015.08.055.
120. Wick, P; Louw-Gaume, A. E.; Kucki, M.; Krug, H. F.; Kostarelos, K.; Fadeel, B.; Dawson, K. A.; Salvati, A.; Vazquez, E.; Ballerini, L.; Tretiach, M.; Benfenati, F.; Flahaut, E.; Gauthier, L.; Prato, M.; Bianco, A. Classification Framework for Graphene-Based Materials. *Angew. Chem. Int. Ed.*, **2014**, *53*, 7714–7718. doi:10.1002/anie.201403335.
121. Nawaz, K.; Khan, U.; Ul-Haq, N.; May, P.; O'Neill, A.; Coleman, J. N. Observation of Mechanical Percolation in Functionalized Graphene Oxide/Elastomer Composites. *Carbon*. **2012**, *50*, 4489–4494. doi:10.1016/j.carbon.2012.05.029.
122. Ozbas, B.; O'Neill, C. D.; Register, R. A.; Aksay, I. A.; Prud'homme, R. K.; Adamson, D. H. Multifunctional Elastomer Nanocomposites with Functionalized Graphene Single Sheets. *J. Polym. Sci. Part B Polym. Phys.* **2012**, *50*, 910–916. doi:10.1002/polb.23080.
123. Lape, N. K.; Nuxoll, E. E.; Cussler, E. L. Polydisperse Flakes in Barrier Films. *J. Membr. Sci.* **2004**, *236*, 29–37. doi:10.1016/j.memsci.2003.12.026.
124. Groover M. P. *Fundamentals of Modern Manufacturing*. Materials, Processes, and Systems: Michael McDonald, USA, 2010.
125. Mabry, M.; Rumpf, F.; Podobnik, I.; Westveer, S.; Morgan, A.; Chung, B.; Andrews, M. Cabot Corporation: Methods for Producing Elastomeric Compositions, US6040364A, 2000.
126. Crank, J. ed: *Diffusion in polymers*. Academic Press: London, 1977.
127. Klopffer, M.-H.; Flaconneche, B. Transport Properties of Gases in Polymers: Bibliographic Review. *Oil Gas Sci. Technol.* **2001**, *56*, 223–244. doi:10.2516/ogst:2001021.

128. Dhoot, S. N.; Freeman, B. D.; Stewart, M. E. Barrier Polymers. In Encyclopedia of polymer science and technology; Kroschwitz, J. I., Eds.; New York: Wiley-Interscience, **2003**; Vol. 5; pp. 193–263.
129. Kim, H.; Miura, Y.; Macosko, C. W. Graphene/Polyurethane Nanocomposites for Improved Gas Barrier and Electrical Conductivity. *Chem. Mater.* **2010**, *22*, 3441–3450. doi:10.1021/cm100477v.
130. Song, S. H.; Kim, J. M.; Park, K. H.; Lee, D. J.; Kwon, O.-S.; Kim, J.; Yoon, H.; Chen, X. High Performance Graphene Embedded Rubber Composites. *RSC Adv.* **2015**, *5*, 81707–81712. doi:10.1039/C5RA16446J.
131. Yan, N.; Buonocore, G.; Lavorgna, M.; Kaciulis, S.; Balijepalli, S. K.; Zhan, Y.; Xia, H.; Ambrosio, L. The Role of Reduced Graphene Oxide on Chemical, Mechanical and Barrier Properties of Natural Rubber Composites. *Compos. Sci. Technol.* **2014**, *102*, 74–81. doi:10.1016/j.compscitech.2014.07.021.
132. Gan, L.; Shang, S.; Jiang, S. Impact of Vinyl Concentration of A Silicone Rubber on The Properties of The Graphene Oxide Filled Silicone Rubber Composites. *Compos. Part B Eng.* **2016**, *84*, 294–300. doi:10.1016/j.compositesb.2015.08.073.
133. Yang, M.; Tian, M.; Jia, Q.-X.; Shi, J.-H.; Zhang, L.-Q.; Lim, S.-H.; Yu, Z.-Z.; Mai, Y.-W. Improved Mechanical and Functional Properties of Elastomer/Graphite Nanocomposites Prepared by Latex Compounding. *Acta Mater.* **2007**, *55*, 6372–6382. doi:10.1016/j.actamat.2007.07.043.
134. Yang, X.; Giese, U.; Schuster, R. H. Characterization of Permeability of Elastomers, Part I – Hnbr. *Kautsch. Gummi Kunststoffe*. **2008**, *61*, 294–300.
135. Yang, X.; Schneider, L. K. A.; Giese, U.; Schuster, R. H. Characterization of Permeability of Elastomers, Part Ii. *Kautsch. Gummi Kunststoffe*. **2010**, *63*, 496–505.
136. Ha, H.; Park, J.; Ha, K.; Freeman, B. D.; Ellison, C. J. Synthesis and Gas Permeability of Highly Elastic Poly(Dimethylsiloxane)/Graphene Oxide Composite Elastomers using Telechelic Polymers. *Polymer*. **2016**, *93*, 53–60. doi:10.1016/j.polymer.2016.04.016.
137. Cui, Y.; Kundalwal, S. I.; Kumar, S. Gas Barrier Performance of Graphene/Polymer Nanocomposites. *Carbon*. **2016**, *98*, 313–333. doi:10.1016/j.carbon.2015.11.018.
138. Nielsen, L. E. Models for the Permeability of Filled Polymer Systems. *J. Macromol. Sci. Part – Chem.* **1967**, *1*, 929–942. doi:10.1080/10601326708053745.
139. Bharadwaj, R. K. Modeling the Barrier Properties of Polymer-Layered Silicate Nanocomposites. *Macromolecules*. **2001**, *34*, 9189–9192. doi:10.1021/ma010780b.
130. Gusev, A. A.; Lusti, H. R. Rational Design of Nanocomposites for Barrier Applications. *Adv. Mater.* **2001**, *13*, 1641–1643. doi:10.1002/1521-4095(200111)13:21%3c1641::AID-ADMA1641%3e3.0.CO;2-P.
141. Fredrickson, G. H.; Bicerano, J. Barrier Properties of Oriented Disk Composites. *J. Chem. Phys.* **1999**, *110*, 2181–2188. doi:10.1063/1.477829.
142. Cussler, E. L.; Hughes, S. E.; Ward, W. J.; Aris, R. Barrier Membranes. *J. Membr. Sci.* **1988**, *38*, 161–174. doi:10.1016/S0376-7388(00)80877-7.
143. Dunkerley, E.; Schmidt, D. Effects of Composition, Orientation and Temperature on the O 2 Permeability of Model Polymer/Clay Nanocomposites. *Macromolecules*. **2010**, *43*, 10536–10544. doi:10.1021/ma1018846.
144. Sadasivuni, K. K.; Ponnamma, D.; Kim, J.; Thomas, S. eds: *Graphene-Based Polymer Nanocomposites in Electronics*. Springer International Publishing: Cham, 2015**.**
145. Paul, D. R.; Robeson, L. M. Polymer Nanotechnology: Nanocomposites. *Polymer*. **2008**, *49*, 3187–3204. doi:10.1016/j.polymer.2008.04.017.
146. Kumar, V.; Hanel, T.; Galimberti, M.; Giese, U. Graphene / Styrene Butadiene Rubber Nanocomposite. *Kautsch. Gummi Kunststoffe*. **2014**, *9*, 29–36.
147. Kumar, V.; Hanel, T.; Giannini, L.; Galimberti, M.; Giese, U. Graphene Reinforced Synthetic Isoprene Rubber Nanocomposites. *Kautsch. Gummi Kunststoffe*. **2014**, *67*, 38–46.
148. Giese, U.; Fleck, F.; Möwes, M. M.; Dilman, T.; Klüppel, M.; Hanel, T. "Graphene Filled Nitrile Butadiene Rubber Nancomposites". *Kautsch. Gummi Kunststoffe*. **2015**, *67*, 69–79.
149. Schopp, S.; Thomann, R.; Ratzsch, K.-F.; Kerling, S.; Altstädt, V.; Mülhaupt, R. "Functionalized Graphene and Carbon Materials as Components of Styrene-Butadiene Rubber Nanocomposites

Prepared by Aqueous Dispersion Blending: Functionalized Graphene and Carbon Materials as Components". *Macromol. Mater. Eng.* **2014**, *299*, 319–329. doi:10.1002/mame.201300127.
150. Wu, J.; Xing, W.; Huang, G.; Li, H.; Tang, M.; Wu, S.; Liu, Y. "Vulcanization Kinetics of Graphene/Natural Rubber Nanocomposites". *Polymer*. **2013**, *54*, 3314–3323. doi:10.1016/j.polymer.2013.04.044.
151. Mao, Y.; Wen, S.; Chen, Y.; Zhang, F.; Panine, P.; Chan, T. W.; Zhang, L.; Liang, Y.; Liu, L. "High Performance Graphene Oxide Based Rubber Composites". *Sci. Rep*. **2013**, *3*, 2508. doi:10.1038/srep02508.
152. Potts, J. R.; Shankar, O.; Murali, S.; Du, L.; Ruoff, R. S. "Latex and Two-Roll Mill Processing of Thermally-Exfoliated Graphite Oxide/Natural Rubber Nanocomposites". *Compos. Sci. Technol.* **2013**, *74*, 166–172. doi:10.1016/j.compscitech.2012.11.008.
153. Zhao, X.; Zang, C.; Wen, Y.; Jiao, Q. "Thermal and Mechanical Properties of Liquid Silicone Rubber Composites Filled with Functionalized Graphene Oxide". *J. Appl. Polym. Sci.* **2015**, *132*, 42582. doi:10.1002/app.42582.
154. Wang, C.; Liu, Z.; Wang, S.; Zhang, Y. "Preparation and Properties of Octadecylamine Modified Graphene Oxide/Styrene-Butadiene Rubber Composites Through an Improved Melt Compounding Method". *J. Appl. Polym. Sci.* **2016**, *133*, 42907.
155. Wang, L.; Zhang, L.; Tian, M. "Effect of Expanded Graphite (Eg) Dispersion on the Mechanical and Tribological Properties of Nitrile Rubber/Eg Composites". *Wear*. **2012**, 276–277, 85–93. doi:10.1016/j.wear.2011.12.009.
156. Potts, J. R.; Shankar, O.; Du, L.; Ruoff, R. S. "Processing–Morphology–Property Relationships and Composite Theory Analysis of Reduced Graphene Oxide/Natural Rubber Nanocomposites". *Macromolecules*. **2012**, *45*, 6045–6055. doi:10.1021/ma300706k.
157. Cho, D.; Lee, S.; Yang, G.; Fukushima, H.; Drzal, L. T. "Dynamic Mechanical and Thermal Properties of Phenylethynyl-Terminated Polyimide Composites Reinforced With Expanded Graphite Nanoplatelets". *Macromol. Mater. Eng.* **2005**, *290*, 179–187. doi:10.1002/mame.200400281.
158. Bokobza, L. "Elastomeric Composites Based on Nanospherical Particles and Carbon Nanotubes: A Comparative Study". *Rubber Chem. Technol.* **2013**, *86*, 423–448. doi:10.5254/rct.13.86983.
159. Payne, A R. "*Reinforcement of elastomers*". Wiley & Sons: New-York, 1965**.**
160. Kim, J. S.; Yun, J. H.; Kim, I.; Shim, S. E. "Electrical Properties of Graphene/Sbr Nanocomposite Prepared by Latex Heterocoagulation Process at Room Temperature". *J. Ind. Eng. Chem.* **2011**, *17*, 325–330. doi:10.1016/j.jiec.2011.02.034.
161. Araby, S.; Meng, Q.; Zhang, L.; Kang, H.; Majewski, P.; Tang, Y.; Ma, J. "Electrically and Thermally Conductive Elastomer/Graphene Nanocomposites by Solution Mixing". *Polymer*. **2014**, *55*, 201–210. doi:10.1016/j.polymer.2013.11.032.
162. Mu, Q.; Feng, S. "Thermal Conductivity of Graphite/Silicone Rubber Prepared by Solution Intercalation". *Thermochim. Acta*. **2007**, *462*, 70–75. doi:10.1016/j.tca.2007.06.006.
163. Heinrich, G.; Basak, G. C. eds: "*Advanced rubber composites*". Springer: Heidelberg, New York, 2011**.**
164. Dreyer, D. R.; Bielawski, C. W. "Graphite Oxide as an Olefin Polymerization Carbocatalyst: Applications in Electrochemical Double Layer Capacitors". *Adv. Funct. Mater.* **2012**, *22*, 3247–3253. doi:10.1002/adfm.201103152.
165. Gangopadhyay, R.; De, A. "Conducting Polymer Nanocomposites: A Brief Overview". *Chem. Mater.* **2000**, *12*, 608–622. doi:10.1021/cm990537f.
166. Bauhofer, W.; Kovacs, J. Z. "A Review and Analysis of Electrical Percolation in Carbon Nanotube Polymer Composites". *Compos. Sci. Technol.* **2009**, *69*, 1486–1498. doi:10.1016/j.compscitech.2008.06.018.
167. Zhan, Y.; Lavorgna, M.; Buonocore, G.; Xia, H. "Enhancing Electrical Conductivity of Rubber Composites by Constructing Interconnected Network of Self-Assembled Graphene with Latex Mixing". *J. Mater. Chem.* **2012**, *22*, 10464–10468. doi:10.1039/c2jm31293j.
168. Munson-McGee, S. H. "Estimation of the Critical Concentration in An Anisotropic Percolation Network". *Phys. Rev. B.* **1991**, *43*, 3331–3336. doi:10.1103/PhysRevB.43.3331.
169. Kim, H.; Macosko, C. W. "Processing-Property Relationships of Polycarbonate/Graphene Composites". *Polymer*. **2009**, *50*, 3797–3809. doi:10.1016/j.polymer.2009.05.038.

170. Kim, H.; Macosko, C. W. "Morphology and Properties of Polyester/Exfoliated Graphite Nanocomposites". *Macromolecules*. **2008**, *41*, 3317–3327. doi:10.1021/ma702385h.
171. Araby, S.; Zhang, L.; Kuan, H.-C.; Dai, J.-B.; Majewski, P.; Ma, J. "A Novel Approach to Electrically and Thermally Conductive Elastomers Using Graphene". *Polymer*. **2013**, *54*, 3663–3670. doi:10.1016/j.polymer.2013.05.014.
172. Guimont, A.; Beyou, E.; Alcouffe, P.; Cassagnau, P.; Serghei, A.; Martin, G.; Sonntag, P. "Pentadecane Functionalized Graphite Oxide Sheets as a Tool for the Preparation of Electrical Conductive Polyethylene/Graphite Oxide Composites". *Polymer*. **2014**, *55*, 22–28. doi:10.1016/j.polymer.2013.11.049.
173. Wei, T.; Song, L.; Zheng, C.; Wang, K.; Yan, J.; Shao, B.; Fan, Z.-J. "The Synergy of A Three Filler Combination in the Conductivity of Epoxy Composites". *Mater. Lett.* **2010**, *64*, 2376–2379. doi:10.1016/j.matlet.2010.07.061.
174. Boland, C. S.; Khan, U.; Backes, C.; O'Neill, A.; McCauley, J.; Duane, S.; Shanker, R.; Liu, Y.; Jurewicz, I.; Dalton, A. B.; Coleman, J. N. "Sensitive, High-Strain, High-Rate Bodily Motion Sensors Based on Graphene–Rubber Composites". *ACS Nano*. **2014**, *8*, 8819–8830. doi:10.1021/nn503454h.
175. Romasanta, L. J.; Hernández, M.; López-Manchado, M. A.; Verdejo, R. "Functionalised Graphene Sheets as Effective High Dielectric Constant Fillers". *Nanoscale Res. Lett.* **2011**, *6*, 508. doi:10.1186/1556-276X-6-508.
176. Wu, J.; Huang, G.; Li, H.; Wu, S.; Liu, Y.; Zheng, J. "Enhanced Mechanical and Gas Barrier Properties of Rubber Nanocomposites with Surface Functionalized Graphene Oxide at Low Content". *Polymer*. **2013**, *54*, 1930–1937. doi:10.1016/j.polymer.2013.01.049.
177. Kumar, S. K.; Castro, M.; Saiter, A.; Delbreilh, L.; Feller, J. F.; Thomas, S.; Grohens, Y. "Development of Poly(Isobutylene-Co-Isoprene)/Reduced Graphene Oxide Nanocomposites for Barrier, Dielectric and Sensingapplications". *Mater. Lett.* **2013**, *96*, 109–112. doi:10.1016/j.matlet.2013.01.036.
178. Wu, S.; Tang, Z.; Guo, B.; Zhang, L.; Jia, D. "Effects of Interfacial Interaction on Chain Dynamics of Rubber/Graphene Oxide Hybrids: A Dielectric Relaxation Spectroscopy Study". *RSC Adv*. **2013**, *3*, 14549–14559. doi:10.1039/c3ra41998c.
179. Hernández, M.; Bernal, M.; del, M.; Verdejo, R.; Ezquerra, T. A.; López-Manchado, M. A. "Overall Performance of Natural Rubber/Graphene Nanocomposites". *Compos. Sci. Technol.* **2012**, *73*, 40–46. doi:10.1016/j.compscitech.2012.08.012.
180. Tian, M.; Zhang, J.; Zhang, L.; Liu, S.; Zan, X.; Nishi, T.; Ning, N. "Graphene Encapsulated Rubber Latex Composites with High Dielectric Constant, Low Dielectric Loss and Low Percolation Threshold". *J. Colloid Interface Sci.* **2014**, *430*, 249–256. doi:10.1016/j.jcis.2014.05.034.
181. Singh, V. K.; Shukla, A.; Patra, M. K.; Saini, L.; Jani, R. K.; Vadera, S. R.; Kumar, N. "Microwave Absorbing Properties of a Thermally Reduced Graphene Oxide/Nitrile Butadiene Rubber Composite". *Carbon*. **2012**, *50*, 2202–2208. doi:10.1016/j.carbon.2012.01.033.